KINETIC STUDIES OF CATION EXCHANGE REACTIONS OF II-VI QUANTUM DOTS

By

Adekunle Titus Akinmola

A Thesis Submitted in Partial Fulfillment of the Requirements for the Degree of Master of Science in Chemistry

Middle Tennessee State University
December 2019

Thesis Committee:

Dr. P. Greg Van Patten, Research advisor

Dr. Andrienne Friedli

Dr. Charles C. Chusuei

Dr. Justin Miller

ABSTRACT

The quest to synthesize excellent materials with qualities ranging from size-tunability, photoluminescence quantum yield and storability has led to the study of cation exchange reaction as one of the many methods explored. Cation exchange reactions have been heavily studied with CdSe as starting materials to synthesize Ag_2Se quantum dots (QDs) and other QDs. In this work, ZnSe QDs has been studied and successfully used as a starting material for cation exchange for Ag_2Se QDs. The reaction was carried out at room temperature with cheap and readily available materials. Kinetics of reaction was studied to understand the rate of cation exchange reaction using ZnSe compared to known and heavily studied CdSe QDs. The fitting of the kinetic curves was done with multiple exponential function with fastest rate constant (*k*) value 1.9×10^2 s^{-1} obtained for ZnSe and a later slower reaction rate, which is the reverse for CdSe. It is understood that the cation exchange at the surface process for ZnSe system was faster, but the interior exchange process inside the crystal was slower. The observed rates are due to shorter bond length and stronger bonds in ZnSe QDs. How ligands on the surface of CdSe QDs affect the rate of exchange with Ag^+ ion was investigated. CdSe QDs were treated with hexadecylamine (HDA), trioctylamine (TOA), dodecylamine (DDA), oleylamine (OlAm), stearate, and oleate as capping ligands. The amines show difference in their rate constant (*k*) values with DDA being the fastest, followed by OlAm, HDA, and TOA being the slowest. This trend is attributed to the basis of steric effect of these ligands

preventing diffusion of ions in and out of QD in the solution. Oleate and stearate have similar chain-length (C18), but show different exchange rate constant k_1, with oleate (1.8×10^3 s^{-1}) being faster than 3.8×10^2 s^{-1} observed with stearate. These rates are attributed to steric hindrance caused by these ligands on the surface of the QDs, which is consistent with the trend observed with the amines.

TABLE OF CONTENTS

LIST OF TABLES

1. INTRODUCTION

1.1 Motivation and Goals

This thesis describes work aimed at improving our understanding and control of cation exchange reactions in quantum dot materials. Cation exchange is a process that allows transformation of one quantum dot material into another, and it has been shown as a promising route to quantum dot materials that are difficult to make by standard, direct methods. There are two main objectives related to this work, and they are reflected in three specific aims. The two objectives are (1) to demonstrate cation exchange reactions that employ environmentally-friendly Zn^{2+} cations instead of Pb^{2+} and Cd^{2+} in the quantum dot starting materials, and (2) to better understand whether ligands can play an important role in the rates of cation exchange reactions. These objectives lead to the following specific aims of this research:

i. to demonstrate the use of Zn^{2+} in room temperature cation exchange reactions of metal chalcogenide quantum dots;

ii. to compare rates of cation exchange reactions when Zn^{2+} is substituted for Cd^{2+} in these reactions;

iii. to investigate the effects of ligands on the rates of cation exchange reactions.

This work builds on previous work in our laboratory that has shown that room temperature cation exchange can be used as a practical, scalable method for

producing high-quality QDs starting with CdSe, CdS, and PbS quantum dots. The present work aims to use the principles and methods described in that previous work to incorporate ZnSe as a starting material to produce other metal selenide quantum dots. Stopped-flow absorbance measurements are also employed to study cation exchange kinetics for the first time.

1.2 Quantum Dots

Quantum Dots (QDs) are semiconductor nanocrystals with diameters ranging from 1 to 10 nm, and which have properties that differ from the corresponding bulk substance. In fact, in the nanometer size range, many of the properties are dependent on the size of the QD. Among the most important size-dependent properties are electronic properties, which also affect optical and chemical properties. The electronic properties change with size in these nano-sized particles due to quantum size effects, which will be explained in the next section. The changes in the electronic energy levels with size lead to changes in light absorption and emission, and also lead to changes in oxidation-reduction potentials for these materials.

These size-dependent properties make QDs interesting for a number of applications different from their bulk counterparts. Some applications that have driven interest in QDs include bio-imaging,[1] solar cells, and luminescent displays.[3,4,5] QDs are used in bio-imaging due to their extremely small size, strong light absorption, photostability, and intense emission. These characteristics may

make them good alternatives to molecular-based dyes that are currently used in bio-imaging. QDs are good candidates for solar cells because of the tunability of the energy levels with size, their strong light absorption, their photostability, and due to certain phenomena, such as multi-exciton generation, which have been claimed in QDs, but are not possible in bulk materials. QDs have already been commercialized in luminescent displays, in particular in Samsung's Q-LED televisions.[6] In these devices, QDs have made the colors and brightness better in certain spectral ranges, but future Q-LED TV's are expected to use QDs exclusively as light emitting materials.

Synthesis and manipulation of nanomaterials present special difficulties compared with bulk (macroscopic) samples. QDs are generally handled as colloidal suspensions in liquid solution, embedded in glasses, or attached to substrate surfaces. For our studies, we have been primarily interested in colloidal suspensions in liquid because these types of QDs can be prepared in large quantities and then easily removed from the reaction mixture and processed for use in the types of applications described above. For colloidal suspensions in liquid, the QD synthesis requires the ability to control the size of the product quantum dots. Size control, in turn, requires a delicate balance between precursor reactivity, precursor concentration, the binding of surfactant molecules (called capping ligands) to the surfaces of the growing quantum dots, and the reaction temperature. The reaction must also be carried out in a suitable solvent mixture that is stable at the desired temperature and can dissolve all of the reaction

components. In some cases, it may be very difficult or impossible to find conditions that allow synthesis of a given type and size of QD.

1.2.1 Properties of QDs

The size of quantum dots has been an essential property that makes them differ from their bulk materials. The difference in the properties of QDs and its bulk is due to quantum size effect which brought about the name quantum dots. Quantum size effect is caused by the confinement of electrons within the particles with sizes smaller than their bulk counterparts. The confinement explains the electronic, optical, and chemical properties of the quantum dots which are the major properties that distinguish the quantum dots from their corresponding bulk materials.

The optical and electronic properties of the quantum dots explain their luminescence and energy levels which is also determined by the size of the particles. Size range of particles relates to the change in electronic and optical properties caused by the presence of the particle boundaries.

The changes in the energy spectra are reflected in the properties of QDs and the way quantum dots interact with light. Quantum dots absorb light which leads to excitation of an electron in the particle from the valence to the conduction band. The excited electron leaves a positively charged hole behind. The hole acts like a particle with its own mass and charge. This excited electron-hole pair is

called an exciton. The excited electron and hole can recombine as the electron returns to its ground state. The exciton's energy is emitted as light giving rise to photoluminescence.

Quantum dots emit different colors of light and the corresponding luminescence and absorbance spectra of the particles undergo continuous shifting throughout the visible and near infrared regions depending on the particle size.[7] Figure 1.1 is showing typical absorbance spectra of CdSe QDs with absorbance peaks at different wavelength depending on the particle size.

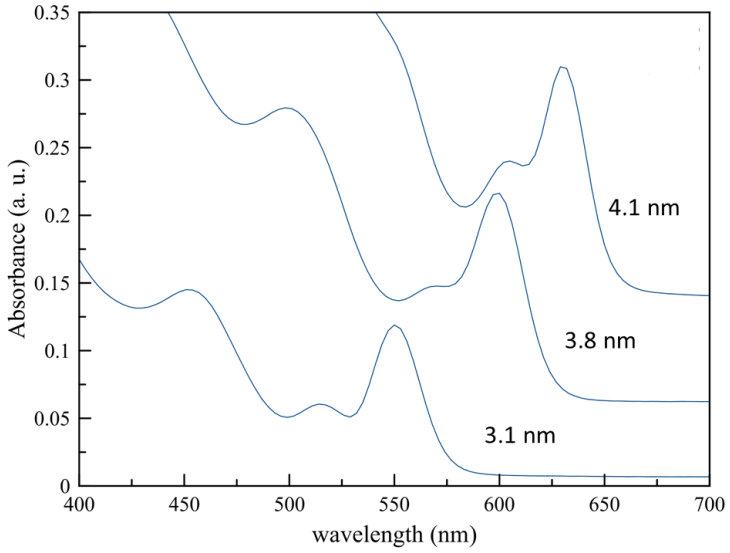

Figure 1.1. Absorbance spectra of CdSe QDs of different particle sizes.

The energy of the photon emitted as light also known as the QD's band gap energy can better be explained as the sum total of the band gap of the bulk material

(i.e. the band gap energy between the valence and conduction band), the confinement energy of the excited electron and the positively charged hole. This is illustrated below in Figure 1.2.

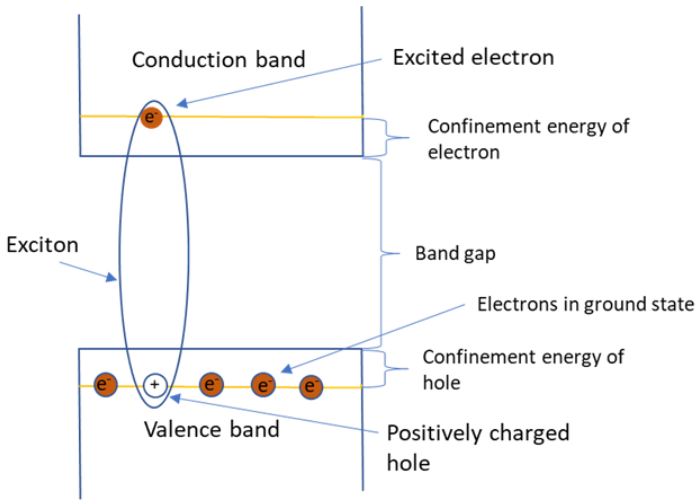

Figure 1.2. Schematic illustration of band gap energy of a semiconductor quantum dot.

Brus developed an effective mass model relating particle size and band gap energy of a semiconductor quantum dot and the bandgap of its bulk material.[8]

$$E_g(qd) = E_g(bulk) + \frac{h^2}{8R^2}\left(\frac{1}{m_e} + \frac{1}{m_h}\right) - \frac{1.8e^2}{4\pi\varepsilon_0\varepsilon R} \quad (1.1)$$

where E_g is the bandgap energy of the quantum dot or bulk solid, m_e is the effective mass of the electrons in the solid, m_h is the effective mass of the hole in the solid, R is the quantum dot radius, and ε is the dielectric constant of the solid. The

bandgap energy postulated by the Brus model, and therefore the confinement energy, depends on the size of the particles. A decrease in the particle size leads to an increase in the bandgap energy of the QDs and vice versa. This is analogous to a particle in a box where the QD is the box and its electron is the particle. The continuous decrease in the size of the box confines the particles to a continuous smaller volume, as the particle exhibits wave-like properties with the lowest energy equal to the first energy state given by[9]

$$E_1 = \frac{\hbar^2 \pi^2}{2mL^2} \tag{1.2}$$

The confinement causes the wavelength of the particle to be shorter and, therefore resulting in a higher energy wave function of the particle. As the QD size decreases below 10 nm, the energy of an electronic transition is expected to increase by up to 1 to 2 eV and is relatively determined by the properties of the bulk material.[7] This is evident in the absorbance and emission spectra of QDs such as CdSe as shown in Figure 1.1. The primary difference in the bandgap energy of QD and its bulk semiconductor is the confinement energy, which is why the bandgap energy of a given quantum dot depends on the properties of the bulk material.

1.2.2 Applications of QDs

The fascinating properties of quantum dots have given rise to their use in a lot of applications, which include colloidal quantum dot solar cells, bioimaging and

displays. Quantum dots are suitable for such applications due to their tunable bandgap.

Investigating the application of QDs in photovoltaic cells has been an interesting and promising area of research for a number of years.[3,4,10] In solar cell application the particles absorb light and form exciton, exciton diffusion, charge separation, and charge transportation to produce current.[11,12] There has been progress on this work with improvement in the conversion efficiency of the solar cells reported this year (2019) to a record high of 16.6%.[13]

Bioimaging is also one of the known applications of quantum dots. A few of the characteristics, including high extinction coefficients and quantum yields, absorbance and emission tunability, and broad excitation windows into the NIR with narrow emission peaks, contributes to the applicability of quantum dots for bioimaging.[1,2,10] The use of quantum dots in biomedical applications including *in vivo* environment requires the quantum dots to be water-dispersible with very low cytotoxicity.[1] Solubility and toxicity are very important properties considered for quantum dots suitable for biological applications.[14] A number of reviews and subsequent work describe the application of QDs for biomedical application.[5,15,16]

Quantum dots have also brought about great improvement in displays, as quantum dots are applied into the production of latest super ultra-high definition (UHD) and QLED TVs. This technology makes use of uniformly-sized quantum dots of 1 to10 nm in diameter to create subtle, accurate colors that give more brightness and high dynamic range (HDR) when compared to other TVs.[6,17] Cd based quantum dots are already applied in displays. However, there are various

investigations going-on, including this work, on how to successfully replace Cd-containing materials with more environmentally friendly materials such as Zn- and In- containing materials, as Cd based nanomaterials are relatively toxic.[18,19]

1.2.3 History of Quantum Dots

Quantum dots are often referred to as “artificial atoms”, which indicates that quantum dots are single object, (freestanding) with discrete electronic states similar to naturally occurring atoms.[41]

The first quantum dots discovered were CuCl QDs, and this was by Ekimov and Onushchenko in 1981.[20] The CuCl QDs were discovered in multicomponent silicate glasses while heating a supersaturated solid solution which contained copper and chlorine compounds. The CuCl quantum dots found were of sizes varying from 2 to 31 nm. Semiconductor quantum dots have been consistently investigated for several years after their discovery to systematically make high quality materials, by improving their known optical and electronic properties and their applications in everyday life.

Ekimov and coworkers developed a method in 1985 using silicate glasses to synthesize CdS, CdSe, PbS, ZnS and Cd_3P_2.[21] Their method permits different sizes as the crystals are grown in a controlled manner with sizes between 10 – 100 angstroms.

Quantum dots then became the term used to address these materials in the year 1988.[22,40] The name quantum dot refers to the ability of the particles to show quantum size effects. At the time, researchers began to investigate quantum dots

not just from the standpoint of basic research, but also exploring the practical applications of the particles.[7]

A crystal growth method involving the deposition of very thin films layer of semiconductor materials on a substrate was another preparation technique developed by Esaki Leo.[23] The technique, referred to as molecular beam epitaxy (MBE), is preferred by physicists as a way to make QDs. A regular structure of rectangular-pyramid-shaped quantum dots was formed on the substrate. To form this structure, the thickness of the deposited material layer gets to a critical value of few monolayers, followed by self-assembly to build up a thin solid film. The disadvantage of MBE method is that it is complex and quite expensive.[24]

In 1986, Lianos and Thomas synthesized cadmium sulfide (CdS) using inverse micelles.[25] They studied the spectroscopic properties of the CdS particles utilizing radius as a parameter of discussion in terms of colloids theory. Steigerwald et al.[26] also explored inverse micelles to make Cadmium selenide (CdSe) particles. Their group synthesized surfactant-stabilized CdSe particle and went further to cap the particles with phenyl groups using phenyl(trimethylsilyl)selenium (PhSeTMS) as the capping agent. They extended the same technique to synthesize cadmium telluride and mercury selenide using $HgCl_2$ as mercury precursor.[26]

Bawendi et al.[27] developed a simple and highly efficient chemical method of synthesis. Their method of quantum dots synthesis has since been referred to as high-temperature colloidal synthesis. This route of QDs production was first used to produce high-quality II-VI (CdSe, CdS, CdTe) semiconductor quantum dots. There is a control of the outcome of the properties of the quantum dots which

include the size, shape, structure, and monodispersity using their method. Other types of quantum dots such as III-V (InP, GaP, and GaAs), II-V (Cd_3P_2) and IV-VI (PbSe) have been successfully synthesized exploring the high-temperature colloidal synthesis.[28] Another main advantage of this procedure is the possibility to carry out large-scale chemical synthesis of structurally perfect colloidal quantum dots with a desired average size and shape.[7]

Bawendi's method created a lot of interest for comprehensive investigation on the synthesis, characterization, and possible practical applications of these materials. There have been different reports exploring different precursors, investigating the effect of different capping ligands on the surface of the quantum dots, and post-synthesis modification of colloidal quantum dots to produce new types of materials with high luminescence quantum yield.[29]

1.3 Synthesis of Quantum dots

The quest to make high-quality quantum dots with properties ranging from photoluminescence quantum yield, size-tunability, storability, and environmentally friendly materials led to the development of many methods for quantum dots synthesis. The methods explored could be classified as physical and chemical methods depending on the procedure and technique used for the synthesis.

An example of a physical method of synthesis is carried out through nucleation and growth of quantum dots through a vapor-phase reaction of molecular or atomic beams with a substrate characterized by relatively high energy, and can be achieved through molecular beam epitaxy.[23,24,30] Molecular

beam epitaxy (MBE) involves the reaction of one or more thermal beams of atoms or molecules with a crystalline surface under high vacuum conditions known as the epitaxial growth technique. The source of the beam could be a solid source where the metal is heated by thermal radiation or electron beam impact. Pinzolits et al.[31] in 1998 grew PbSe quantum dots on PbTe substrate using molecular beam epitaxy. They reported a well-defined particle with pyramidal shape with a triangular base and steep side facets with size distribution of ~7%.

The MBE method was improved on by Alchalabi et al.[32] in the synthesis of PbSe QDs using PbTe quasi-substrates grown on silicon. They were able to achieve particle size distributions as low as ±2%. However, the MBE method requires very complex processes, equipment, ultra-high vacuum environment and materials of high-purity. The complex MBE method can be replaced by other methods of synthesis that are referred to as chemical methods.[7]

A simpler method of synthesis of quantum dots when compared to molecular beam epitaxy in terms of energy and processes required is the micellar synthesis, which is based on a chemical reaction involving intermicellar exchange of reactant, leading to nucleation and growth of quantum dots. This method has been used in the synthesis of different types of quantum dots and was reported by Steigerwald and coworkers in 1988.[26] They were able to successfully synthesize powders of II-VI materials, such as cadmium selenide and mercury selenide. Other groups were able to synthesize other types of quantum dots using reverse micelle synthesis.[34,35]

Another chemical synthesis of quantum dot is high-temperature colloidal synthesis, which was first reported by Murray, Norris and Bawendi.[27] Their method can be described as a chemical reaction that creates an environment that separates the nucleation and growth of quantum dot at relatively high temperature. The addition of a cold precursors into a hot (265 – 300 ^{o}C) solvent favors nucleation, which is then followed by a quick drop in the temperature of the mixture. The drop in the temperature stops the nucleation process, and the temperature was gradually increased to between 230 – 280 ^{o}C for quantum dot growth. This method was used to synthesize CdS, CdSe and CdTe quantum dots with bright tunable luminescence through this simple one-step reaction, referred to as pyrolysis of organometallic precursors, at 300 ^{o}C.[7] The high temperature aided annealing of particles and emergence of relatively defect-free crystal lattice.[36] However, there is a need to search for new high-temperature solvents, ligands, and precursors and the possibility to use the high-temperature method for the synthesis of better quality of II-VI QDs. The possibility to extend the high-temperature colloidal synthesis to III-V (InP, GaAs, InAs) types of QDs was also investigated.[37,38]

There are many semiconductor materials for which direct synthesis mentioned above has not been found, or there has been difficulty in making high-quality materials through direct synthesis. This challenge may be solved through exploring cation exchange reaction as a means to synthesize new materials. Cation exchange will be emphasized with details in this work as our method of fabrication of QD.

1.3.1 Cation Exchange

A number of types of QDs cannot be fabricated through direct synthesis, as quality particles are not accessible by known methods. Therefore, cation exchange is a strategy to compensate for the limitation by increasing the library of possible QDs that can be synthesized. Cation exchange has been studied and applied on various materials belonging to group II metals and group VI anions (chalcogenides), referred to II-VI semiconductors such as CdSe, CdTe, ZnS, and ZnSe. In addition, I-III-V ($AgInS_2$) IV-VI (GeS_2) classes of semiconductors at the nanoscale level have also been studied.[39]

Cation exchange (CE) reaction can simply be referred to as the replacement of cations in the starting QD and maintaining the anion sublattice of the QD, which can undergo a degree of rearrangement. Cation exchange is favored over anion due to cations being generally smaller than anions in a crystal which explains the high diffusion rate of the cations. They diffuse easily within the relatively rigid lattice of the anion. This technique has been explored to synthesize QDs at room temperature through the use of colloidal QDs synthesized through pyrolysis as the starting material.[65] To achieve an exchange, a conducive environment is created for the cations in a semiconductor QDs to be replaced by desired metal ion to form a new type of QDs as illustrated in Figure 1.3. A generic equation for the cation exchange reaction is given as

$$A_xX_{y\ (s)} + M^{n+}{}_{(aq)} \longrightarrow M_xX_{y\ (s)} + A^{n+}{}_{(aq)} \quad (1.3)$$

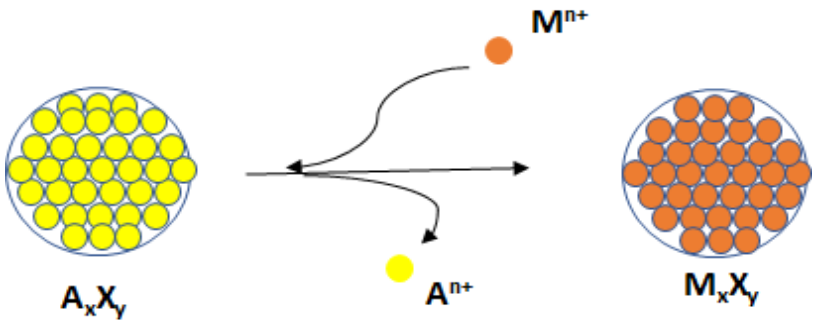

Figure 1.3. Schematic representation of cation exchange reaction. The starting QD with native cations (yellow) are replaced by migrating cations (orange) to produce in type of QD.

In 1993, Mews et al. explored a partial cation exchange reaction of CdS to HgS referred to as QD quantum well system (CdS/HgS/CdS).[33] Their method used $Hg(ClO_4)_2$ as the Hg precursor; which was added with continuous stirring to an aqueous CdS solution. Further addition of precursors of either Hg^{2+} ion or Cd^{2+} ion was done to increase the thickness of the layer of interest.

A complete cation exchange was first successfully reported in 1994 by Zhou et al. for the cation exchange reaction of CdS to PbS in aqueous solution.[42] CdS capped with polyvinylpyrrolidone (PVP) synthesized by their group was used as the starting material. This was followed by adding $Pb(CH_3COO)_2$ into the solution of CdS leading to displacement of Cd in the Cd-S bond by the Pb^{2+} to form a Pb-S bond. They reported a color change with rates of exchange depending on the concentration of the Pb precursor. They also noted that complete exchange of Cd^{2+}

for Pb^{2+} can be achieved in the chemical reaction with an increase in the concentration of Pb^{2+} ion and time of reaction.

Son et al. developed a method for the exchange of CdSe to Ag_2Se and the reverse reaction to CdSe.[43] They suspended CdSe QDs in toluene, which was mixed with $AgNO_3$ dissolved in methanol under ambient temperature. The strong binding ability of methanol to free divalent cations was said to have favored the forward reaction which took place rapidly (~1 s). An immediate color change and complete disappearance of fluorescence were observed in the mixture. X-ray diffraction (XRD) patterns and absorption spectra were used to confirm a complete exchange with the product showing evidence of Ag_2Se. The reverse reaction was also carried out under ambient conditions by mixing Ag_2Se QDs in toluene with the mixture of $Cd(NO_3)_2$ and methanol in the presence of tributylphosphine. A period over 1 minute was observed for the reverse reaction which also showed evidence of complete exchange with XRD and absorption analysis.[43]

Cation exchange in nanowires was investigated using electrical conductivity measurements.[44] This technique involved cation exchange in nanowires in-between electrode pairs. Trizio et al. reported a complete and partial cation exchange reaction using Cu_2Se QDs as the starting materials to make SnSe QDs and Cu_2SnSe_3 alloy materials.[45] Their method explored the use of relatively environmentally friendly materials. However, the method discussed required high temperature (100 ^oC). Other works involving cation exchange have been reported using different starting materials, ligands, and precursors with procedures that required high temperature and toxic reagents.[46,47] The synthesis of new materials

through cation exchange reaction involving environmentally friendly material carried out at room temperature is of great essence, and it's been of interest in this work.

1.3.1.1 Cation Exchange and Thermodynamics

A typical cation exchange equation of reaction as shown in equation (1.3) involves the replacement of A^+ cations in a starting AX QD exposed to a solution of M^+ (metal cation) to produce the MX QD. The equation follows a process that can be divided into four ideal steps as, A-X dissociation, M-X association, M^+ desolvation, and A^+ solvation.[48] The association and dissociation processes correspond to lattice and surface energy of AX and MX QDs. Lattice energy (ΔH_{latt}) is the energy required to break the crystals apart into isolated ions at absolute zero temperature. Solvation and desolvation of A^+ and M^+ energy is determined by the affinity of the exchange cations for both the solvent and ligands involved in the exchange reaction.[39]

The affinity of the cations for the solvent and ligands is understood in terms of Pearson's hard and soft acids and bases (HSAB) theory.[49] The theory helps to determine or suggest the affinity of metal ions to ligands and solvent. Acids and bases are known to characteristically have acceptor and donor atoms respectively. Hard bases are denoted to have donor atoms of low polarizability and high electronegativity which are hard to oxidize; soft bases have donor atoms with high polarizability and low electronegativity, and they are more easily oxidized. Conversely, hard acids have acceptor atoms with high positive charge and small

size, while in soft acids the acceptor atoms have low positive charge and larger size.

Therefore, hard acids have a high affinity for hard bases, while soft acids have a high affinity for soft bases. This also helps to determine the solubility of the cations used in a typical cation exchange reaction. The cations explored in this work are Ag^{+}, Cd^{2+}, and Zn^{2+}, and Ag^{+} is considered a soft Lewis acid when compared to Cd^{2+} and Zn^{2+} as a result of their absolute hardness values reported by Pearson. Table 1.1 shows a list of several cations (acids) and ligands or solvents (bases) used in cation exchange corresponding to absolute hardness.[49]

Table 1.1. Experimental Absolute Hardness, ŋ, of Typical Cations (acids) and Ligands or Bases Applicable in CE Reactions[49]

Acid	**Absolute hardness, *η* (eV)**	**Base**	**Absolute hardness, *η* (eV)**
Cu^{+}	6.28	$C_6H_5NH_2$	4.4
Pd^{2+}	6.75	C_6H_5SH	4.6
Ag^{+}	6.96	C_6H_5OH	4.8
Sn^{2+}	7.94	C_5H_5N	5.0
Cu^{2+}	8.27	$(CH_3)_3P$	5.9
Au^{3+}	8.40	$(CH_3)_2S$	6.0
Pb^{2+}	8.46	$(CH_3)_2P$	6.0
Cd^{2+}	10.29	CH_3CN	7.5
Zn^{2+}	10.88	CH_3Cl	7.5
In^{3+}	13	$(CH_3)_2O$	8.0
Ga^{3+}	17	CH_3F	9.4

η, denotes absolute hardness[49]

1.3.1.2 Ligands in QDs

QDs are made up of an inorganic core which is capped or surrounded with ligands. The ligands are generally organic molecules which provide electronic and chemical capping of surface bonds, and they prevent uncontrolled growth and clustering of QDs as shown in Figure 1.4.

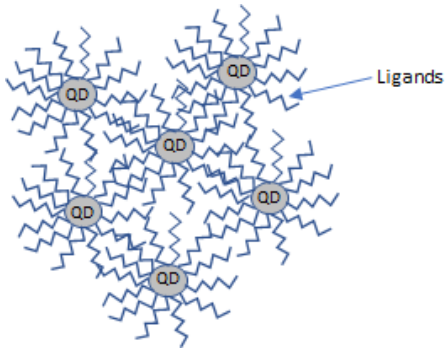

Figure 1.4. Schematic illustration of QDs showing the QDs and positions of the attached ligands

The ligands also aid the solubility and stability of the QDs in a desired environment or solution. They form metal-ligand complexes in the QDs, and as a result stabilize the particles.[50] The stabilizing ligands of QDs could be hydrophobic ligands such as trioctylphosphine (TOP), trioctylphosphine oxide (TOPO), oleic acid (OA), or dodecylamine. They could also contain hydrophilic ligands such as 2-aminoethanethiol, dihydrolipoic acid, L-cysteine, and mercaptopropionic acid.[72]

The polarity of the ligands determines the solubility of the QDs. Therefore, hydrophilic ligands are used in the synthesis of water-soluble QDs and hydrophobic ligands for hydrophobic QDs.[7]

Ligands are generally basic and can be classified as being soft or hard base according to Pearson's hard soft acid and base theory. This property makes ligands play an important role in cation exchange reaction because they behave like Lewis base in the reaction process.[39]

Amines and carboxylates are hard ligands if compared to phosphines and thiols. Thiols are referred to as soft ligands when compared to phosphines with the exception of thioethers such as $(CH_3)_2S$ which show similar hardness values to those of phosphines.[39] They are capable of forming very stable metal-ligand bond with hard and soft acids (cations) respectively. They can form a sigma (σ) bond with the cation by donating their lone pair of electrons. Phosphine can form strong bonds with cations through pi-backbonding, which can be described as the bonding of pi-conjugated ligands to a transition metal. This is because they are good pi(π) acceptor.[39] This entails donation of electrons from a filled pi-orbital or lone pair electrons of the ligands into an empty orbital of the metal, while the metal releases electrons from d-orbital into the empty pi-antibonding orbital of the ligand.

Hard ligands (bases) such as amines and carboxylates form strong bonds with hard acids (cations) such as Zn^{2+} and Cd^{2+} ions in our cation exchange reactions. This served as part of the driving force for the cation exchange reaction of ZnSe and CdSe QDs to Ag_2Se. The role of ligands on the surface of QDs in cation exchange reactions is a major investigation in this work, and it has been

deduced that the rate of a cation exchange reaction can also be determined or altered by the ligands bonded to the surface of the QDs. Ligands serve as a shield for the QDs from external environment as shown in Figure 1.4. Therefore, they affect the rate at which metal ions approaching the QDs during cation exchange gets to the surface of the QDs to prompt the exchange process. The structure of the ligands and their carbon chain length create steric hindrance for the incoming metal ions. Tertiary ligands create more steric hinderance when compared to primary ligands, which results in a slower rate of cation exchange reaction when tertiary ligands are attached to the surface of the original QDs. The part ligands play in the rate of cation exchange reactions with QDs show fascinating results with different ligands (amines and carboxylic acids) studied in this work.

1.3.1.3 Kinetics

The study of the rate of cation reactions was one of the main goals of this work. We were able to investigate the speed of the reactions using the stopped-flow kinetic instrument.

A number of the reactions were very fast at few seconds or less and could be observed with the human eye. However, a stopped-flow instrument with a dead time of 5 milliseconds was used to investigate the exact rate of the cation exchange reaction. The instrument requires change in absorbance of the reacting species to the product formed as it measures the change in absorbance with respect to time. The requirement was met as our typical starting material such as CdSe absorbs only in the visible region while the product (Ag_2Se) absorbs across the visible and

into the near infrared region. All the reagents used during this experiment were hydrophobic, and toluene was chosen as a suitable solvent to fulfil the co-solubility of reagents and reactants essential for the stopped-flow experiment.

The reaction in this experiment was run under pseudo-first order conditions, as the metal ion reagent was prepared to have a concentration ten times that of the QDs. The rate law can be expressed as[51]

$$R \propto k[M^{2+}] \tag{1.4}$$

The rate constant *k* varies for each reaction depending on how fast the reaction occurred. Therefore, the relative value of the rate constant, *k*, helps to understand the difference in the rate of cation exchange with each reaction.

1.3.1.4 Cation Exchange of ZnSe.

ZnSe QDs as a starting material for a cation exchange is a known system that has been studied by different groups. This system can be used as a route to synthesize new materials that are not accessible through the conventional synthetic methods.

Shao et al. studied the partial, sequential and complete cation exchange reactions of ZnSe to make ZnCdSe ternary doped with Cu or Ag and Ag_2Se QDs at room temperature.[52] They carried out their reaction in an aqueous solution using

hydrazine as a suitable Lewis base to promote the forward reaction. However, QD fabricated in an aqueous environment were found to be of lower quality when compared to those made in hydrophobic solvents. Hydrazine is a toxic and explosive chemical used for explosives. Hydrazine which serves as the driving force in their work may require to be handled with much caution owing to the characteristics of the chemical. Furthermore, reported ligands bonded to the surface of the QDs need to be removed through a purification procedure before the exchange reaction can occur, which require a need for selection of suitable purification reagents.[52]

ZnSe QDs have also been used as starting materials for complete exchange with Cd^{2+} and Pb^{2+} ions,[53,54,55] in a hydrophobic environment. These methods explored different precursor compositions, concentrations, and temperatures. However, their reaction procedures required high temperatures (above 100 ^{o}C).

In this thesis, the investigation of a cation exchange method with ZnSe QDs as the starting material at room temperature using cheap, readily available, and relatively environmentally friendly precursors was discussed. The reaction precursors and reagents are easy to handle in open air, and all the reactions were carried out in a hydrophobic environment. Purification of the starting material was not required for the cation exchange reaction to occur. The conditions that drive the cation exchange reaction are discussed in detail. A typical absorbance peak of between 350 to 390 nm was observed for ZnSe QDs used as the starting

material in this work. An example of the absorbance spectrum of ZnSe QDs is shown in Figure 1.5.

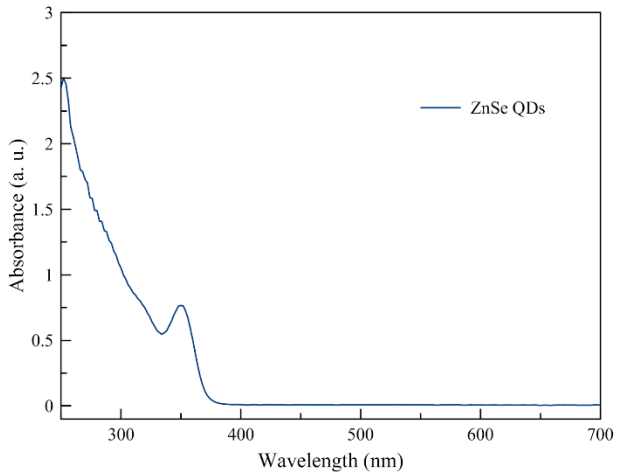

Figure 1.5. A typical absorbance spectrum for ZnSe QD.

1.4 Characterization

1.4.1 Spectrophotometry

UV-VIS-NIR absorbance spectra provides information necessary for characterizing QDs. Absorbance is linked to features of the particles that include the extinction coefficient, size, and concentration of the particles. This is possible because different QDs absorb light of specific energy depending on their composition. The principle is based on the measurement of light absorbed by the

sample, in this case, the QDs solution, in the UV-Vis and IR region. This principle can be explained by the equation of absorbance

$$A = log_{10} \frac{I_0}{I} \quad (1.5)$$

where *A* is the absorbance of the sample, I_0 is the intensity of incident light on the sample, and *I* is the intensity of the transmitted light.

The technique involves a light source, deuterium lamp for UV region and tungsten lamp for Vis region, that passes through the monochromator (prism or diffraction grating) and a narrow slit. The light is then dispersed into an array by a prism or diffraction grating. The monochromatic light with known intensity passes through the sample in the cuvette, and then to the detector. I_0 is the intensity of the monochromatic light entering the sample, while *I* is the intensity of the light emerging from the sample.[56] The absorbance gives information on the extinction coefficient, size, and concentration of the QDs.

1.4.2 Transmission Electron Microscopy (TEM)

The TEM is a microscope with very high resolution for obtaining images of particles in the nanometer scale via the transmission of electron beam through samples at high voltage depending on the capacity of the instrument. The source of the electrons is at the top of the microscope. When the electrons are released, they travel through a vacuum in the instrument focused by lenses into a small beam. Then, the electron beam passes through the sample and strikes a screen

at the bottom of the microscope. The electrons strike the QDs and are scattered. The amount of the electrons scattered is dependent on the density of the sample (i.e. materials made of elements with higher atomic number). The image of the particles is finally formed by the electrons that are not scattered but made their way to the screen at the bottom of the microscope. This technique leverages on the interaction between the electrons and the sample as the beam transmits through the particles.

TEM acquires information on the shape and the size distribution of the QDs. Shape and size of QDs can be monitored before and after treatment (e.g. cation exchange) with TEM images. The sample is prepared using a sample grid of about 3.05 mm in diameter, thickness and mesh size of approximately 100 μm. The sample grid could be made of copper, platinum, or gold, and is covered with a thin carbon film only a few nanometers thick. The sample is deposited onto the carbon film and is introduced to the TEM through a sample holder so that the region of interest on the grid is directed to the path of electron beam. An image is collected at the best region showing a reasonable number of visible particles. Figure 1.6 shows an image of spherical CdSe QDs.

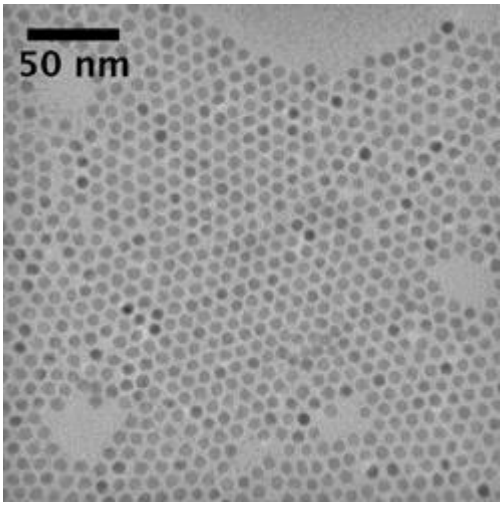

Figure 1.6. TEM image of spherical CdSe QDs.

1.4.3 Powder X-Ray Diffraction

Powder x-ray diffraction (PXRD) allows determination of the microcrystal structure (symmetry and interatomic distances) using X-ray beams. A crystal structure has unit cells built up repeatedly in regular three dimensions. The structure of the crystal is determined from the intensities and direction of the diffracted x-rays. The intensities of the diffracted rays depend relatively on the arrangement of atoms in each unit cell, and the repeat distances between the unit cells.[57] Bragg's law specifies the conditions required for diffraction, enabling calculation of the angle at which constructive interference from x-rays scattered by parallel planes of atoms will produce a diffraction peak.

$$\lambda = 2d \sin\theta \quad (1.6)$$

where wavelength, λ, in most cases is fixed in diffractometers, diffraction peak is produced by parallel planes at a specific angle 2θ. The distance between parallel planes of atoms is designated as d.[57]

1.5 Research Outline

One of the goals of this thesis is to investigate the use of environmentally friendly starting materials for cation exchange reactions at room temperature. Zinc selenide QDs were explored as starting materials to make silver selenide QDs through room temperature cation exchange reaction. ZnSe QDs were synthesized using reported methods of synthesis.[58,59,60,61,62] The use of ZnSe as a starting material was compared to a known system of CdSe QDs, which have soon interesting results as a starting material for cation exchange.[43,65] However, CdSe QDs are toxic materials. Therefore, there is a need to explore the use of environmentally-friendly materials such ZnSe QDs as starting materials with the desire to make quality materials in terms of narrow size distribution, size tunability, photoluminescence quantum yield, and scalability through ZnSe QDs.

The rate of exchange reactions was also studied in the two systems through stopped-flow kinetics measurements. Characterization was carried out for desired properties of the QDs with UV-VIS-NIR absorption spectrometer, TEM, and PXRD.

Secondly, the kinetic study of cation exchange reactions in CdSe QDs coated with different capping ligands was explored. CdSe QDs were synthesized via a previously-reported synthesis,[29] and then further treated with amine and fatty acid ligands including hexadecylamine, oleylamine, dodecylamine, trioctylamine, oleic acid, and stearic acid. The rate of cation exchange of Ag^{+} for Cd^{2+} in the ligand-treated CdSe QDs was investigated with a stopped-flow kinetic instrument. The curves obtained from the rate measurement were fitted using an equation developed to fit the curves. Different rate constant (*k*) values obtained will provide an understanding of the effect of surface ligands in the rate of cation exchange reaction of Ag^{+} for Cd^{2+} in CdSe QDs.

2 EXPERIMENTAL

2.1 Materials

Diethylzinc ($(C_2H_2)_2$)Zn, 95 %), selenium powder (Se, 99.5 %), and tri-n-octylphosphine (TOP, 97 %) were obtained from Strem Chemicals and used as received. Hexadecylamine (HDA, technical grade, 90%), oleylamine (OlAm, technical grade, 70%), octadecene (ODE, technical grade, 90%), zinc oxide (ZnO, ACS grade ≥ 99.0%), mineral oil (paraffin oil, light), octadecylamine (ODA, ≥99%), selenium dioxide (SeO_2, ReagentPlus, power, 99.8%), and oleic acid (OA, technical grade, 90%) were used as received from Sigma-Aldrich. Lauric acid (LA, laboratory grade) was obtained from Flinn Scientific Inc. and used as received. Hexanes (ACS grade), chloroform (ACS grade), toluene (laboratory grade), methanol (ACS grade), and 1-butanol (ACS grade) were obtained and used as received from Fisher Scientific. Silver nitrate ($AgNO_3$, reagent grade, 99.9%) was obtained from Baker & Adamson and used as received. Acetonitrile (dry, water < 10 ppm), hexadecyl hexadecanoate (HH, 98%), tri-n-octylamine (TOA, 97%), and stearic acid (97%) were obtained and used as received from Acros Organics. Absolute ethyl alcohol (200 proof) was obtained and used as received from Pharmco-Aaper. Tetrachloroethylene (TCE, ultrapure, spectrophotometric grade, 99+ %), tributylphosphine (TBP, 95%) and dodecylamine (DDA, 98%) were obtained and used as received from Alfa Aesar. Tetracosane (>99%) was obtained from TCI America and used as received. Cadmium stearate was obtained and used as received from MP Biomedicals Inc.

2.2 Methods

2.2.1 ZnSe QD Synthesis

Five different synthesis using previously-reported methods were investigated towards making high-quality ZnSe QDs.

Synthesis of Laurate-capped ZnSe QDs. The procedure described by Chen et al. used ZnO in lauric acid and Se powder in tri-n-octylphosphine (TOP) as zinc and selenium precursors respectively.[60] The selenium precursor used was prepared in the glovebox. To prepare the precursor, a 5 mL disposable syringe and needle, spatula, weighing paper, a 5 mL sample vial with sizable magnetic stir bar, and a 5 mL glass metal Luer lock air-tight syringe, which included a syringe stopcock and metal needles, were introduced to the glovebox through the antechamber. Using a 4 mL sample vials, 0.39 g (5 mmol) of selenium powder and 2.4 g of TOP were weighed into the sample vial and allowed to stir on the stirrer plate for 30 – 40 minutes in the glovebox.

The reaction was set up by weighing 0.41 g (5.0 mmol) of ZnO, 5.0 g (25 mmol) lauric acid and 1.9 g (8.0 mmol) HDA into a 3-neck round bottom flask with a magnetic stir bar. The middle neck of the flask was fixed to a condenser which was connected to a bubbler and Schlenk line for nitrogen flow and vacuum. One side of the flask was fixed to a temperature probe which was connected to a temperature controller using a glass thermometer adaptor and the other side of the flask was sealed with a rubber septum. All the connections and joints were secured

with plastic Keck clamps. The 3-neck round bottom flask was placed in a heating mantle connected to the temperature controller on a magnetic stirrer plate. The Schlenk line was set for nitrogen gas to go through the bubbler into the reaction mixture. The port was adjusted to achieve a steady stream of bubbles in the bubbler. Then, the temperature was set on the temperature controller to get the temperature of the mixture to 300 ^{o}C. Using an air-tight glass syringe with stopcock, the Se precursor was taken from the 5 mL vial in the glovebox. The precursor was injected swiftly into the flask through the rubber septum at 300 ^{o}C. The temperature of the sample dropped to 280 ^{o}C. Growth of the QDs was carried out at 280 ^{o}C. The duration of crystal growth was between 20 seconds to 30 minutes. The QD sizes were controlled by varying growth time.

Stearate-capped ZnSe QDs. The ZnSe synthesis method reported by Li et al. was also investigated.[59] Li et al developed their method using zinc stearate as their zinc precursor, with stearate and octadecylamine as the capping ligands. Zinc stearate (0.064 g, 0.10 mmol), octadecylamine (0.056 g, 0.20 mmol), 2.1 g tetracosane, and 2.2 g octadecene (ODE) were weighed in open air. The reagents were mixed in a 3-neck round bottom flask with a stir bar. The mixture was heated to 330 ^{o}C using the reaction setup described above for the Chen et al.[60] synthesis under N_2 flow. Selenium precursor was prepared in the glovebox. Apparatus needed for the preparation of the sample was introduced to the glovebox as described in the previous experiment. Selenium powder (0.048 g, 0.6 mmol) was dissolved in 0.20 g tributylphosphine (TBP) and 0.31 g ODE. The selenium stock

was stirred for about 30 minutes to 1 hour in the glovebox. Selenium was swiftly injected into the 3-neck round bottom flask using a glass syringe with stopcock at 330 ºC. The same procedure was repeated at varying injection temperature and QD growth time to optimize the procedure.

HDA-capped ZnSe QDs. The procedure described by Hines and Guyot-Sionnest was also followed for the synthesis of ZnSe QDs.[58] They investigated ZnSe QDs synthesis using diethylzinc as a zinc precursor and HDA as the capping ligand. HDA (18 g) was weighed in a 3-neck round bottom flask. The flask was kept under vacuum for one hour at 130 ºC to dry and degas the HDA. To achieve this, the Schlenk line setup was arranged as described above for the Chen et al. experiment, and the port was opened to the vacuum where the pump vacuumed out the air in the flask at a temperature of 130 ºC with continuous stirring. After an hour, the pressure within the apparatus was reduced to 100 mTorr or less. After this, the flask was switched to nitrogen flow, and the HDA was then heated to 310 ºC under nitrogen. Zinc and selenium precursors were prepared in the glovebox. The preparation involved using a 1 mL disposable syringe to measure and add 0.80 mL diethylzinc to 1.0 mL TOPSe (1 M) which was prepared by dissolving selenium powder in TOP. The precursor was further diluted with 4.0 mL TOP using a 5 mL disposable syringe. The Zn/Se solution was injected into the hot HDA solution at 310 ºC, and the growth temperature was set at 270 ºC with growth time varying from 5 minutes to 3 hours.

Oleate-capped ZnSe QDs. Shen et al. prepared ZnSe QDs using a three part method.[62] First, the stock solution of zinc precursor was prepared by mixture of ZnO (0.16 g, 2 mmol), oleic acid (2.3 g, 8 mmol), and paraffin oil (19 mL). The mixture was loaded in a 3-neck round bottom flask and placed under vacuum to obtain a pressure within the apparatus of 100 mTorr and below. The flask was then heated to 300 ^{o}C with continuous stirring under a nitrogen flow until the solution became colorless. Selenium precursor was made by adding SeO_2 (0.22 g, 0.002 mol) and 20 mL of octadecene in a 3-neck flask. The mixture was degassed by heating to 240 ^{o}C for 10 minutes under air in the hood. The synthesis was carried out by mixing 2.0 mL of the Se precursor and 5.0 mL of paraffin oil in a 3-neck flask. The solution was heated to 300 ^{o}C under a nitrogen gas flow. Then, 2.0 mL of Zn precursor solution was rapidly injected into the hot solution at 300 ^{o}C. QD growth was carried out at 280 ^{o}C for 5 minutes and longer times, depending on the desired size of the QDs.

ODA-capped ZnSe QDs. A final method that was investigated was one reported by Groeneveld et al.[61] They followed a procedure similar to the one reported by Hines and Guyot-Sionnest, however, they used a different capping ligand for their synthesis. Hines used HDA as the capping ligand while Groeneveld used ODA in their synthesis. The synthesis was carried out by weighing ODE (1.9 g) and ODA (0.55 g) into a 3 neck round bottom flask with a stir bar. The flask was fixed to a condenser which was connected to a bubbler and Schlenk line for nitrogen flow and vacuum. A temperature probe and rubber septum were fixed to

the remaining two necks of the flask. The mixture was heated to a temperature of 290 ^{o}C using a heating mantle connected to the temperature controller. Diethylzinc and selenium powder were used as precursors for zinc and selenium respectively. Diethylzinc (0.4 M) stock solution was prepared in the glove box with a mixture of 0.25 g diethylzinc with 5.0 mL ODE. Selenium stock solution was prepared by dissolving 0.40 g selenium powder in 5.0 mL TOP. A glass syringe with stopper and metal needle was used to collect 0.50 mL zinc stock and 1.0 mL selenium stock mixture. This was followed by a quick injection of the syringe contents into the hot solution in the flask. After the injection, the temperature was reduced to 270 ^{o}C for QD growth for 30 minutes. The temperature was removed after 30 minutes, and absorbance of the sample was analyzed on the UV-Vis spectrophotometer.

2.2.1.1 Purification of ZnSe QDs

The purification methods reported alongside synthesis methods described by the groups mentioned above were investigated with a few changes as the reported purification methods did not work effectively. A mixture of solvents was used to induce flocculation, which was then centrifuged to precipitate the QDs.

Oleate-capped ZnSe QDs was purified with a mixture of polar solvents to precipitate out hydrophobic ZnSe QDs. To purify, 0.25 mL ZnSe QD sample was added to 0.25 mL hexanes, 0.050 mL oleic acid, 0.50 mL butanol, and 0.50 mL ethanol in a 2 mL centrifuge tube. A pipettor was used for all measurements. The mixture was vortexed. The polar mixture of ethanol and butanol was expected to

cause the particles to fall out of the solution mixture. However, the alcohols did not mix well with the hydrophobic particles. Therefore, hexane was added to enhance the miscibility of the solution, thus allowed the particles to fall out of the solution. The cloudy solution was then centrifuged to precipitate the QDs. After centrifugation, the supernatant was checked to see if it still had particles. A clear and colorless supernatant indicated that approximately all the particles were stuck to the bottom of the 2 mL centrifuge tube. Clear and colorless supernatant was decanted, and the precipitate was re-suspended in desired solvent for cation exchange or other analysis.

2.2.2 Preparation of Silver Exchange Reagent

Silver reagent for cation exchange was prepared as described by Morris et al.[65] The preparation was done in ambient conditions with no effort to prevent it from exposure to air. Silver nitrate (0.56 g) was weighed on an analytical balance into a clean 25 mL beaker and 1.5 mL acetonitrile (CH_3CN) was added to dissolve the salt. The beaker was placed on a stirrer plate with a stir bar in the mixture. The silver nitrate solution was stirred continuously until a homogeneous solution was formed. This was followed by the addition of 8.5 mL of oleylamine and 5.0 mL of toluene. The entire silver reagent solution was stirred for a few more minutes for homogeneity and stored in a reagent bottle. Our silver reagent was kept in an incubator at a temperature of 35 ^{o}C to avoid coagulation or solidification of the solution. The concentration of the reagent was calculated to be 0.22 M, assuming a total volume of 15 mL.

2.2.3 Cation Exchange of ZnSe QDs with Ag^+ ion

Cation exchange of zinc for silver was investigated using ZnSe synthesized from the methods by Hines et al.[58] and Shen et al.[62] This exchange reaction was carried out at room temperature, and there was no attempt to protect the reaction from exposure to air. ZnSe QDs (QDs), (0.25 mL) were purified using the method described in the purification section above. It was kept on the bench to dry and was then dissolved in 0.25 mL toluene in a 2 mL centrifuge tube. A pipettor was used to measure Ag^+ reagent (0.25 mL) prepared as described in section 2.2.2 and was added to the purified ZnSe in the centrifuge tube. The Zn:Ag concentration ratio was kept at 1:10 for all experiments. The highest possible concentration of Zn in the QDs was estimated to be 0.021 M by calculating the concentration of Zn ion in the total amount of Zn-precursor added to the reaction mixture when synthesizing the ZnSe QDs as described in section 2.2.1. Concentration of the silver reagent was calculated to be 0.22 M. High concentration of the Ag resulting to large amount of Ag^+ ions was targeted at pushing for a complete ion exchange of lower concentration Zn ion for Ag ion in the exchange reaction. The reaction mixture turned from yellowish to a dark color immediately after the silver reagent was introduced. The centrifuge tube was agitated manually for about one minute to enhance complete cation exchange reaction. The dark solution observed was a clear indication of the presence of silver selenide (Ag_2Se) QDs in the reaction mixture.

2.2.3.1 Purification of Ag_2Se

Silver selenide was purified using the principle of polar and nonpolar solvents to flocculate the QDs followed by centrifugation. Purification was done at ambient conditions without measures to prevent exposure to air. Acetonitrile (0.50 mL) was added to the final exchange reaction mixture (0.50 mL), which turned the solution turbid. The solution was agitated and centrifuged at 1000 x g for 1 minute, resulting in the particles stuck at the bottom of the tube leaving a clear and colorless supernatant. The supernatant was decanted, then the tube was placed upside down on a Kim wipe on the bench to drain all the liquid in the tube. Particles stuck in the tube were resuspended in 0.25 mL hexane, followed by adding in a mixture of polar solvents. Butanol (0.25 mL) and 0.25 mL methanol were added to flocculate the particles, making the QDs fall out of the solution. The mixture was vortexed and centrifuged at 4000 x g for 3 minutes. If the supernatant was not completely colorless, a few drops of methanol were added until the supernatant became cloudy. Then, the mixture was slightly agitated and spun again at the same centrifuge setting. The clear and colorless supernatant was decanted, and the precipitate was resuspended in either tetrachloroethylene (TCE) for UV-Vis-NIR absorbance or chloroform for PXRD sample preparation.

2.2.4 Synthesis of Cadmium Selenide QDs

Colloidal synthesis of CdSe QDs was carried out as reported by Wu et al.[29] The method involves the rapid injection of a selenium precursor into a solution of cadmium stearate and octadecene, with coordinating ligands at high temperature.

Selenium powder (0.079 g) was dissolved in 2.5 mL trioctylphosphine in the glovebox. The selenium solution was stirred for 30 min or more for the selenium powder to completely dissolve in the mixture. Cadmium stearate (0.068 g), hexadecyl hexadecanoate (0.11 g), hexadecylamine (1.1 g), and octadecene (5.0 g) were weighed into a 25 mL 3-neck round bottom flask. The flask was set up on a Schlenk line as described in the synthesis of ZnSe in section 2.2.1. The reaction flask was then heated to 200 ^{o}C for 30 min under nitrogen gas. The heating was done to dry and degas the mixture in the reaction flask. The reaction temperature was then increased to between 265 to 320 ^{o}C under nitrogen, depending on the desired size of particles. A metal syringe with stopper was used to quickly inject the selenium precursor into the hot, continuously-stirred cadmium stearate solution at 280 ^{o}C. There were gradual color changes in the reaction pot with time after the rapid injection of the selenium precursor. The reaction was stopped after 10 min by removing the heating mantle and placing a water bath under the flask. A number of different sizes of particles can be obtained by varying the Cd:Se molar ratio and TOPSe injection temperature in the range of 265 – 320 ^{o}C. Large particles are generally favored by increasing the growth time, raising the reaction injection temperature, and increasing the Cd:Se molar ratio.

2.2.4.1 Purification of CdSe QDs

CdSe QDs were purified using the same principle reported in section 2.2.3.1 to flocculate and centrifuge the mixture using polar and nonpolar reagents. Ethanol (0.25 mL, 200 proof) was added to synthesized CdSe (0.25 mL) in a 2 mL

centrifuge tube and vortexed. The tube was spun at 17,000 × g for 3 minutes. There were two layers of supernatant and precipitate (particles), and the supernatant was decanted. Precipitated particles were resuspended in 0.25 mL toluene and vortexed for the particles to completely dissolve in the solution. Then, 0.25 mL ethanol was added and mixed. The mixture was centrifuged at same rotation per minute and time. A complete precipitation of the particles was not achieved as the supernatant was not clear. Ethanol (5 drops) was added and manually agitated gently to avoid getting the precipitate back into the supernatant. The tube was spun at the same rotation and time. This was repeated with another five drops of ethanol and spinning until the supernatant was clear and colorless. The clear supernatant was decanted and the CdSe particles were resuspended in toluene and chloroform for cation exchange reaction and absorbance experiments respectively. The purification process was carried out in the lab at room temperature, without measures to prevent exposure to air.

2.2.5 Exchange of Cadmium for Silver

Cation exchange reaction was carried out in ambient temperature with no measures of preventing the exposure of the particles to air. Silver reagent was prepared using the method described in section 2.2.2. Purified 0.25 mL CdSe QDs dissolved in toluene were kept in a 2 mL centrifuge tube. Silver reagent (0.25 mL) was swiftly added to the tube and vortexed for complete mixture of the solution. A quick color change from orange to black was observed.

2.2.5.1 Purification of Ag_2Se

Ethanol (0.50 mL, 200 proof) was added to the exchanged reaction mixture (0.50 mL). The mixture was vortexed and centrifuged at 17,000 × g for 3 minutes. The supernatant was decanted, and the precipitate was dissolved in 0.25 mL toluene. Ethanol was added to the particles solution and spun at the same number of rotations per minute and time. The purification step was repeated one more time and the particles were suspended in TCE for absorbance experiment.

2.2.6 Treatment of CdSe with Ligands

Cadmium selenide QDs was synthesized using the method reported by Wu et al.[29] The CdSe QDs (0.25 mL) were purified as discussed above using polar and nonpolar solvents mixture for flocculation and centrifuged. Purified CdSe QDs were resuspended in 0.25 mL toluene. The consequences of ligands treatment on the QDs was tested by introducing 0.050 mL of each ligand. Ligands investigated include oleic and stearic acids, hexadecylamine, dodecylamine, trioctylamine, and oleylamine. All the ligands were introduced into different purified CdSe QD samples (0.25 mL) in a 2.0 mL centrifuge tube. HDA, stearic acid, and dodecylamine are solid at room temperature. The solid ligands were slightly heated to their melting point. A pipetman was used to add 0.050 mL of the ligands into the QDs and vortexed for complete mixture. The solution was kept in the cabinet for approximately twelve hours. Ligand treated solutions of CdSe QDs were not further purified.

2.2.7 Preparation of ZnSe, CdSe, and Ag^+ reagent for kinetics

The concentration of Zn present in the synthesized ZnSe was calculated to be ≤0.021 M. CdSe as synthesized had a concentration of ≤0.11 M. Silver reagent prepared as described in section 2.2.2 has concentration at least ten times higher than that of the synthesized QDs. The concentration ratio of Zn/Cd:Ag for the cation exchange reaction was ≤1:10 respectively. High concentration of Ag^+ ion was employed to increase the chances of a complete cation exchange of Ag^+ ions for Cd^{2+} or Zn^{2+} ions in the QDs.

QDs and the silver reagent solutions were each diluted ten times from their original concentrations. The concentration ratio of 1:10 was kept for the stopped-flow kinetic experiment to achieve a pseudo-first order reaction.

2.3 Characterization

2.3.1 UV-Vis-NIR Absorbance

A refurbished Cary 14 spectrophotometer (Olis Inc.) was used to collect the absorbance data. Samples were prepared by first purifying the synthesized and exchanged QDs using the corresponding procedures described in sections above. Typically, 0.25 mL of each sample was purified, allowed to dry, and then suspended in solvent. Toluene or chloroform was used as a solvent for CdSe, while hexane was a typical solvent for ZnSe, and tetrachloroethylene (TCE) was used for Ag_2Se QDs. They were then diluted with the same solvent to 3 mL and

transferred into a cuvette. The cuvette was then placed in the spectrophotometer for analysis.

Spectra were recorded for ZnSe QDs in the range of 300 nm to 800 nm. CdSe spectra were recorded over the range of 400 to 700 nm. Exchanged Ag_2Se spectra were obtained over the range of 400 nm to near infrared 1800 nm.

Information obtained from the UV-Vis-NIR spectra can be used to calculate and obtain some properties of the materials synthesized. The wavelength of the lowest energy excitonic peak and the volume of the sample prepared for the UV-Vis experiment are used to calculate the concentration of Cd ions in each QDs reaction batch synthesized. This calculation is done using a series of equations.

The photon energy corresponding to the wavelength of the lowest energy excitonic peak can be obtained using equation 2.1

$$E = \frac{hc}{\lambda} \tag{2.1}$$

where *E* is the photon energy in joules, *h* is Planck's constant, *c* is the speed of light in *m/s*, and *λ* is wavelength in m. Energy calculated in joules was converted to electron volt (*eV*) using equation 2.2.

$$eV = 1.602 \times 10^{-19} J \tag{2.2}$$

The size of the particles, in diameter (D), was obtained using the equation developed by Yu et al.[63] (equation 2.3).

$$D(\mathrm{nm}) = (1.6122 \times 10^{-9})\lambda_a^4 - (2.6575 \times 10^{-6})\lambda_a^3 + (1.6242 \times 10^{-3})\lambda_a^2 - (0.4277)\lambda_a + 41.57 \quad (2.3)$$

where λ_a is the wavelength of the lowest energy absorbance peak.

Yu et al.[63] also developed a mathematical expression for extinction coefficient per mole of particles.

$$\varepsilon = 1600\,\Delta E(D)^3 \quad (2.4)$$

where *E* is the energy in *eV*, and *D* is the diameter of a given particle.
Therefore, the concentration of the QDs can be calculated using Beer-Lambert's law.

$$A = \varepsilon c l \quad (2.5)$$

In equation 1.11, *A* is the absorbance at the peak position of the lowest energy absorbance peak for a given sample, $\boldsymbol{\varepsilon}$ is the extinction coefficient

obtainable with equation 1.10, *c* is the concentration of the QDs and *l* is the path length in cm which is typically 1 cm.

A custom Python script designed to perform these calculations for CdSe QDs was used to obtain properties. Information such as concentration, extinction coefficient, and particle size were obtained through the script by providing the wavelength of the absorbance peak and volume of sample analyzed.

2.3.2 Transmission Electron Microscopy (TEM)

Samples for TEM experiments were prepared without measures to prevent exposure to air. Synthesized 0.25 mL QDs was purified using the procedure described in the purification sections. The purified particles were left to dry for a few minutes. Then, the crystals were resuspended in 3.0 mL toluene. A micro centrifuge tube was used for further dilution using 1.0 mL of toluene added to 0.10 mL of the already diluted QDs. A 1 mL syringe was used to deposit one drop of the diluted QDs onto a 300-mesh copper TEM grid with carbon coating. A pair of forceps was used to hold the TEM grid until the QDs solution droplet on the grid was dry. Once the toluene drop evaporated, the TEM grid was placed on a filter paper in a petri dish and allowed to completely dry for a few hours. The TEM grid was then transferred to a sample holder to be transported to the TEM room for analysis. Transmission electron microscopy analysis was carried out using Hitachi H-7650 operating at 100 kV located in the MTSU Interdisciplinary Microanalysis

and Imaging Center (MIMIC). The TEM instrument was operated and all samples analyzed by Dr. P. G. Van Patten.

2.3.3 Powder X-Ray Diffraction

A relatively large quantity of the sample is required for PXRD compared to other characterization experiments. Samples of synthesized QDs (2.0 mL each) to be analyzed were purified following the purification steps described in the purification sections. The purified samples were left on the workbench to dry for a few minutes. Purified and dried samples were suspended in 0.50 mL chloroform and vortexed. The sample in chloroform solution was dispensed in drops onto a specially-cut, zero background Si XRD blank sample plate. Each drop was left to dry as the chloroform evaporated in the hood, and additional drops were added until all the sample was transferred to the sample plate.

A Rigaku Miniflex 600 X-ray diffractometer was used to analyze the samples at 1 degree per minute scanning a range of angles from 20 to 90 (2θ) degrees.

2.3.4 Stopped-Flow Kinetics

An Applied Photophysics SX20 model stopped-flow instrument was used to collect kinetic information of the cation exchange reactions. The stopped-flow instrument was operated, and data collected by Dr. Justin Miller. Analyzed samples were prepared via the procedure described above. Toluene was used as the solvent for the experiment. Toluene was used to clean the instrument's mixer and syringes to avoid contamination from previous experiments on the instrument.

The experiment was carried out with the instrument temperature set at 25 ^{o}C, and other parameters such as slit width and pathlength was 1 mm and 10 mm respectively. The stopped-flow instrument was set to collect a minimum of 10 replicates for every sample analyzed at every run. All data points were collected with logarithmic time spacing. Silver reagent was diluted 10 times to a concentration of 0.022 M and was injected using syringe B. QD samples for the exchange reaction were also diluted 10 times to maintain the concentration ratio of the synthesized QDs to silver reagent at 1:10. The QD samples were injected into the stopped-flow instrument using syringe A. A schematic diagram of the stopped-flow instrument is shown in Figure 2.1. Pseudo-first order reaction was achieved for the kinetic experiment with the concentration ratio of QD to Ag^{+} reagent of 1:10.

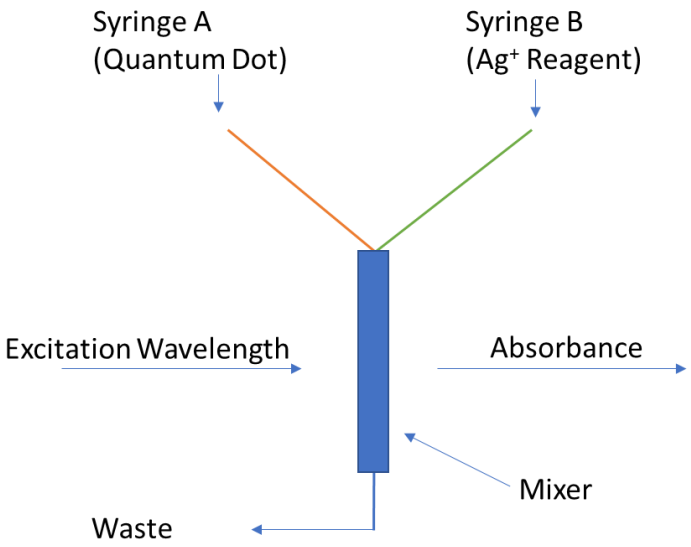

Figure 2.1. Schematic diagram of a stopped-flow kinetic instrument.

3 ZnSe QDS SYNTHESIS AND COMPARISON OF ZnSe AND CdSe QDS AS STARTING MATERIAL

3.1 ZnSe QDs

3.1.1 Laurate-capped ZnSe QDs

Chen et al.[60] synthesized ZnSe QDs with only lauric acid as the coordinating ligand on the surface of the QDs, which in theory, requires a 1:2 ratio of Zn to lauric acid. However, evaporation of lauric acid was observed at high temperature. To synthesize a highly crystalline QD, an elevated temperature typically above 250^{o} C is required for the synthesis. Therefore, HDA with a high boiling point of 330^{o} C was used as cosolvent with lauric acid. HDA served as a coordinating surfactant in the synthesis reaction. Figure 3.1 shows the absorbance spectrum of the laurate-capped ZnSe QDs. The absorbance peak at 409 nm gives an evidence that ZnSe QDs were made in the reaction. The particles can be assumed to be large due to the relatively long wavelength of 409 nm absorbance peak. A relatively broad peak shown here can also be associated to a broad size distribution of the particles synthesized. The purification steps reported in the literature failed to yield pure particles in our experiments. Several purification techniques, which include precipitation using polar and nonpolar solvents and varying the ratio of solvents to sample were explored. Spinning time and speed on the centrifuge were also varied in an attempt to get the particles to fall out of the solution. Due to the failure to obtain sufficiently pure QD material, further studies on the QDs prepared by this

method were not carried out. No attempts were made to determine the QD size distribution or to study cation exchange reactions with these ZnSe QDs.

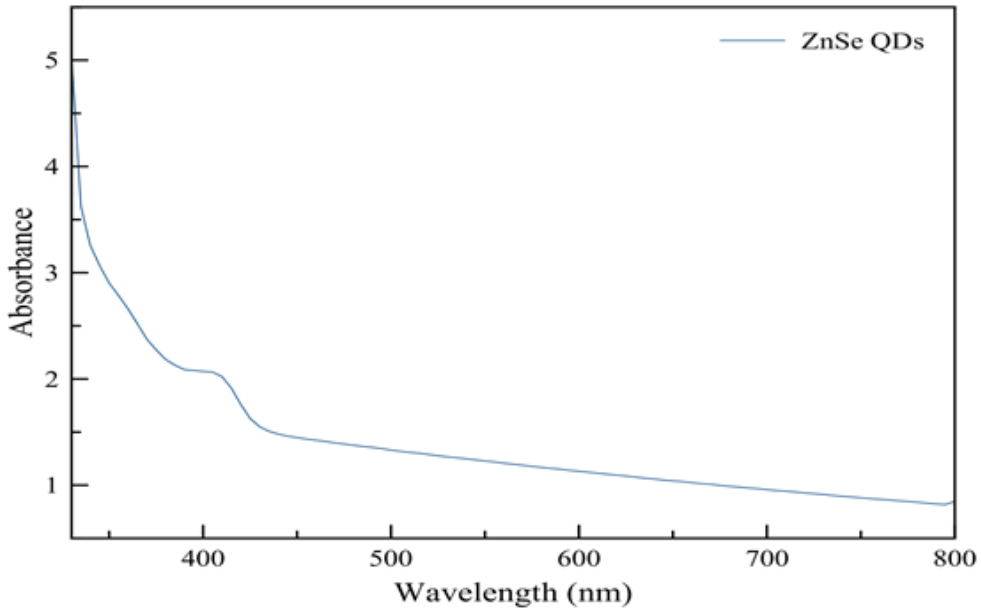

Figure 3.1. Absorbance spectrum of laurate-capped ZnSe QDs.

3.1.2 Stearate-capped ZnSe QDs

Li et al.[59] reported the development of a new synthesis approach for ZnSe QDs using noncoordinating solvent for injection solution of selenium precursor. Octadecene (ODE), which is a noncoordinating solvent, was used to dissolve the selenium precursor. To allow the very high temperature required for the formation of ZnSe, tetracosane mixed with ODE was used as the reaction solvent.

Tetracosane has a boiling point >350^{o} C, making it suitable for reactions even above the ODE boiling point of 315^{o} C. Figure 3.2 shows the UV-visible absorbance spectrum obtained from the stearate-capped ZnSe QDs sample. A 0.25 mL sample was collected from the reaction flask and diluted in 3 mL hexane. No exciton absorbance peak was observed in the UV-visible spectrum of the sample, suggesting that no ZnSe particles were formed. The synthesis was repeated to make sure every reported steps were followed during the synthesis. However, we were never able to find evidence in the absorbance spectrum for the presence of ZnSe QDs.

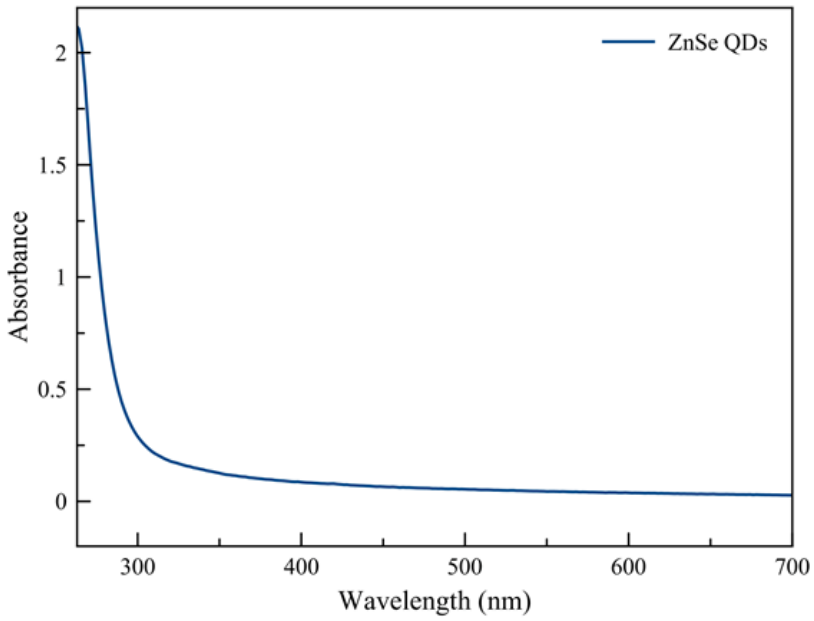

Figure 3.2. UV-visible absorption of putative stearate-capped ZnSe QDs. The spectrum shows no absorbance peak to confirm the presence of ZnSe QDs in the sample.

3.1.3 HDA-capped ZnSe QDs

Figure 3.3 shows an absorbance spectrum of HDA-capped ZnSe QDs. The absorbance peak at 365 nm corresponds to the exciton peak for ZnSe. This peak is a good indication that ZnSe particles were formed in the reaction synthesis. Hines and Guyot-Sionnest[58] reported some conditions that favor the synthesis of high-quality ZnSe QDs to include the ligand and solvent choice. They also considered solubility of the QDs and colloidal stability as part of the properties of high-quality materials. HDA, used as ligand in their reaction, was a suitable alkylamine due to its high boiling point of 330 ºC. Temperature employed is an important parameter for the reaction synthesis due to its effects on the nucleation, growth, and control of particle size during the synthesis.

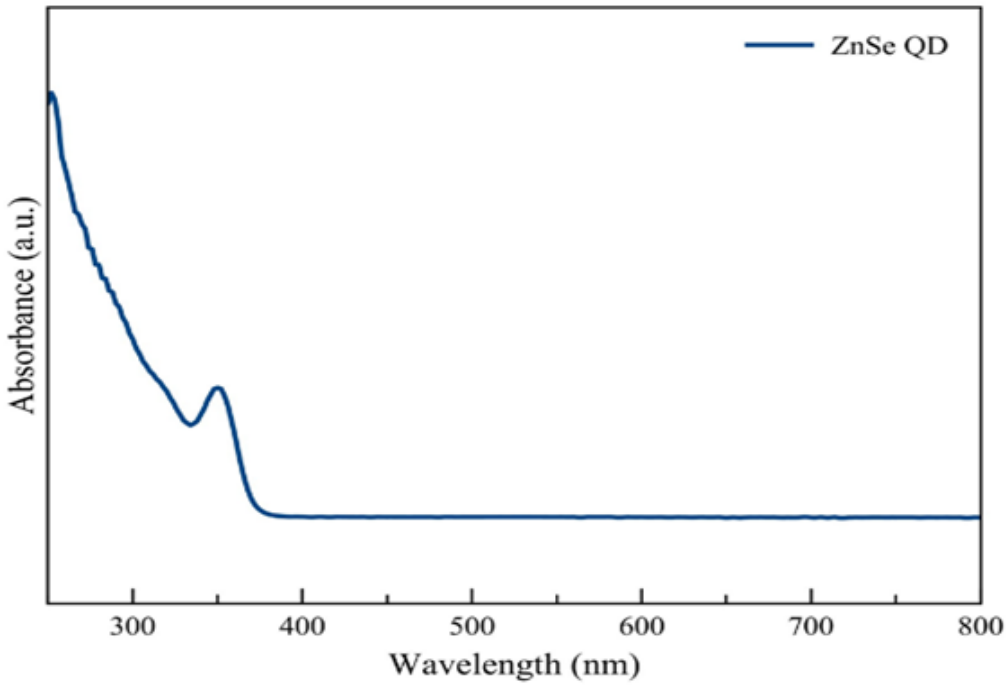

Figure 3.3. UV absorption spectrum of HDA-capped ZnSe QDs.

TEM was used to study the shape and determine the size of the particles. Figure 3.4(a) shows the TEM image of the HDA-capped QDs. It can be inferred from the image that the ZnSe QDs are nearly spherical in shape, and they are not uniform in size. TEM images give the actual particle size and the size distribution can be analyzed using a histogram as shown in Figure 3.4(b). This figure shows the size of the particles was evaluated to be 5.1 nm with standard deviation of 1.5 nm. A narrow absorbance peak observed at about 350 nm in Figure 3.3 connotes relatively smaller and a narrow or uniform size of particles different from what is seen on the TEM image. This could be as a result of the highest population of particles below the size our TEM instrument could detect. Particles of such tiny sizes will require a high-resolution transmission electron microscopy (HRTEM).

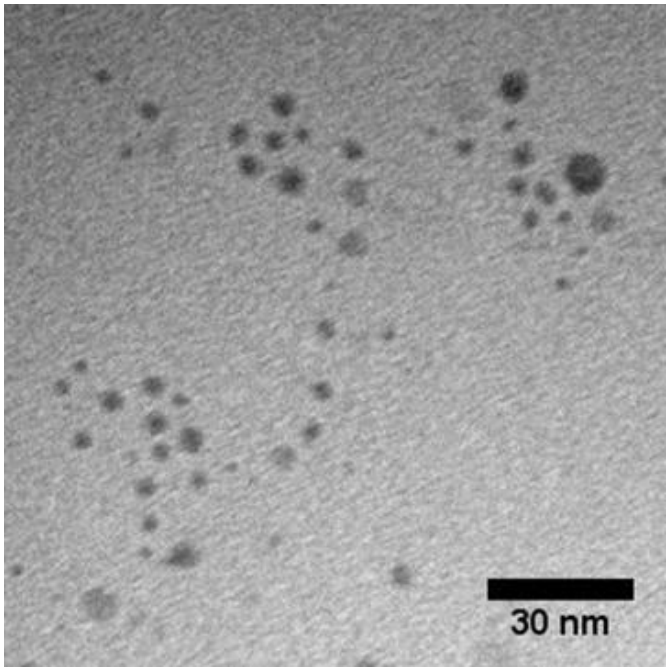

a.

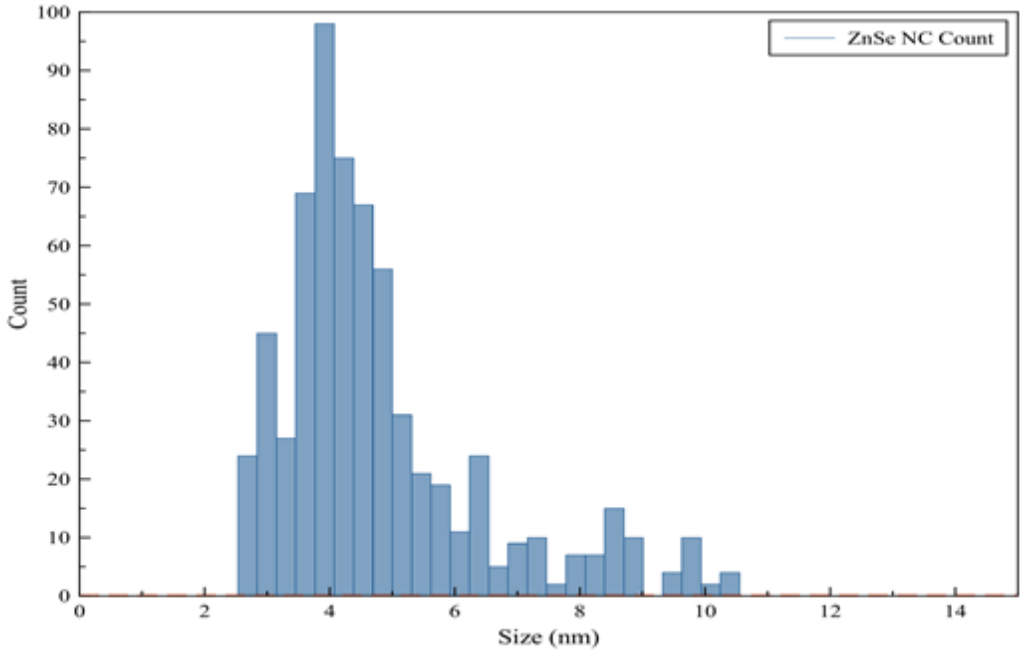

b.

Figure 3.4. (a) TEM image showing HDA-capped ZnSe QDs, and (b) Histogram showing the size distribution of the HDA-capped ZnSe QDs.

Figure 3.5 shows the result from PXRD measurement on the HAD-capped ZnSe QDs. This provides information on the crystal structure of the ZnSe QDs. The three major diffraction peaks shown on the figure correspond to a cubic zinc-blende structured ZnSe particle.[64] The PXRD pattern provides conclusive evidence that we have been able to make ZnSe QDs.

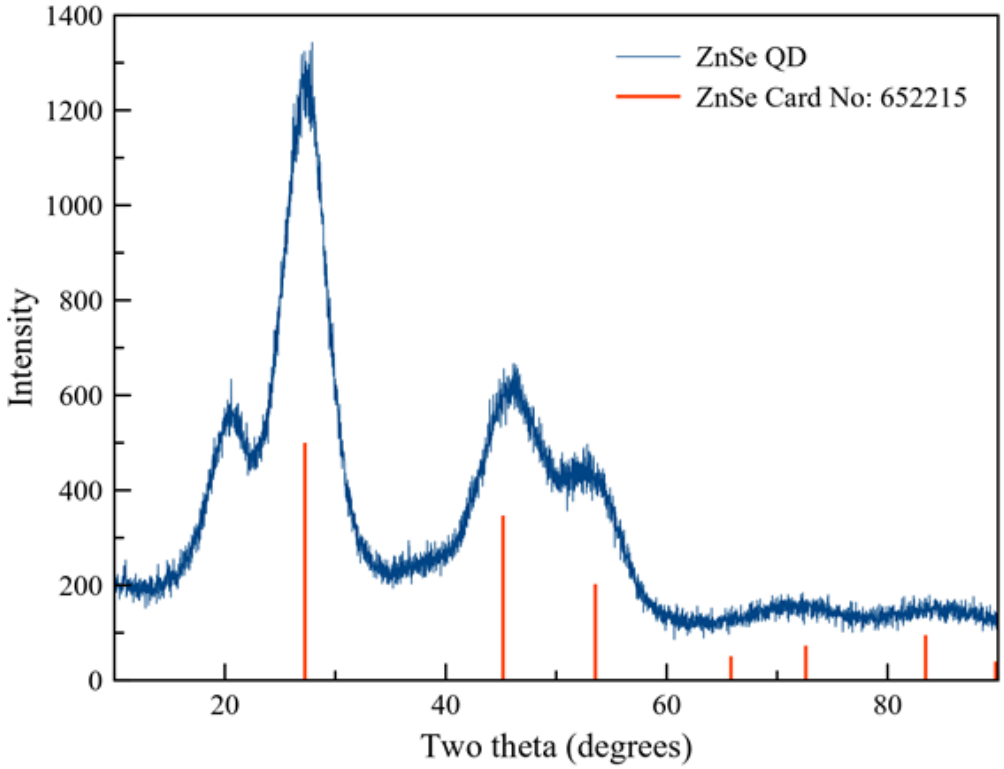

Figure 3.5. HDA-capped ZnSe QDs X-ray diffraction peaks.

3.1.4 Oleate-capped ZnSe QDs

A method that cuts out the use of phosphines and amines in the synthesis of ZnSe QDs was reported by Shen et al.[62] In this procedure, ZnO was dissolved in oleic acid and paraffin oil at high temperature under nitrogen flow, and octadecene as a solvent for SeO_2 which served as the chalcogenide precursor. Both Zn and Se precursors were prepared at elevated temperature in separate flasks. Their primary goal was to make high quality ZnSe QDs with cheap and 'green' reagents. They explored the use of relatively nontoxic and readily available

precursors and solvent (paraffin oil). The high boiling point of paraffin oil makes it suitable for ZnSe QDs synthesis, which requires elevated temperature for high quality materials. Figure 3.6 shows the absorption spectrum of the product obtained by this method. The absorbance peak at 390 nm provides evidence for the presence of ZnSe QDs.

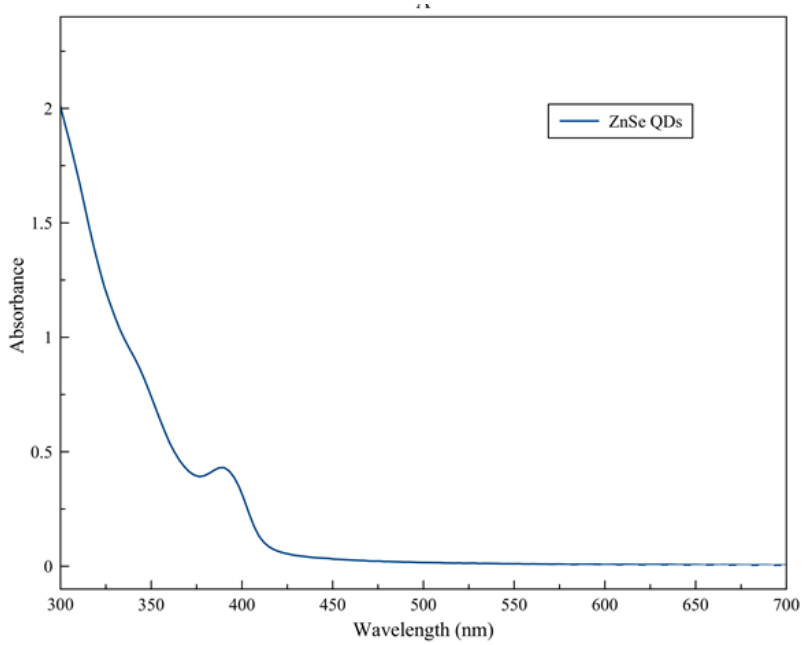

Figure 3.6. UV-visible absorbance spectrum of oleate-capped ZnSe QDs showing an absorbance peak at 390 nm.

The purification process described by Shen et al.[62] was carried out to remove the unreacted Zn and Se precursors present in the reaction mixture. Using acetone as an anti-solvent, as reported in their work, failed to cause precipitation

of the QDs. Instead, two layers of immiscible liquids were formed in the centrifuge tube at every attempt. The ratios of sample, nonpolar solvent, and polar anti-solvent were varied in an attempt to precipitate the QDs. Eventually, it was possible to drive all the QDs into the liquid phase (supernatant), leaving the unreacted precursors and reaction by-products as residues at the bottom of the centrifuge tube. The supernatant was collected and used for further experiments.

Figure 3.7a is a TEM image of oleate-capped ZnSe QDs. The image shows relatively spherical particles with a mean diameter of 4.5 nm and a standard deviation of 0.5 nm. Multiple images of the synthesized ZnSe QDs were analyzed to study the size distribution of the QDs plotted in the histogram in Figure 3.7b.

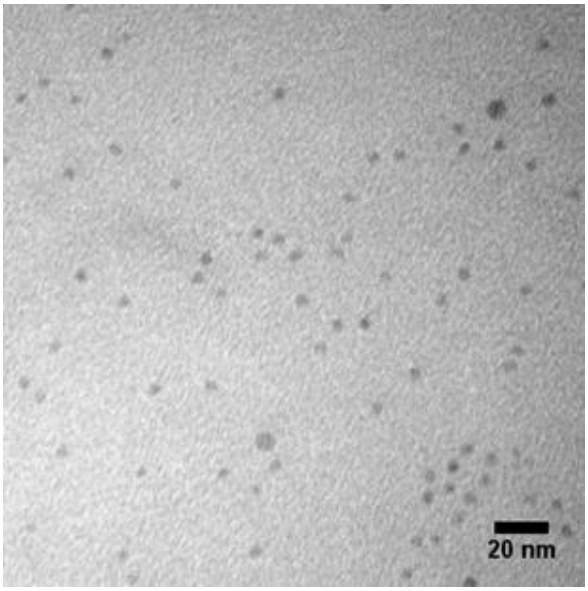

a.

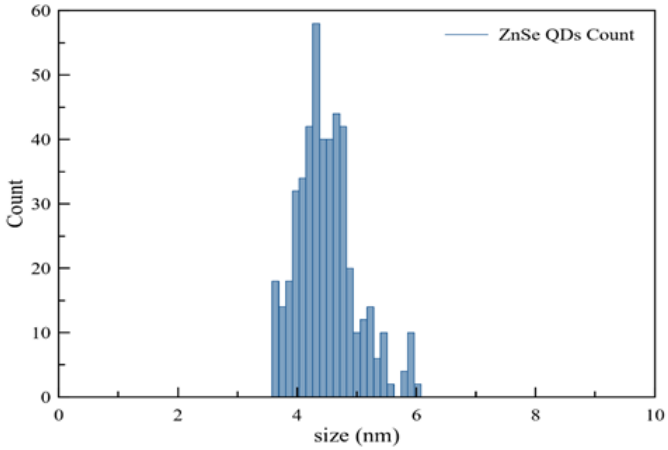

b.

Figure 3.7. (a) TEM image obtained from oleate-capped ZnSe QDs sample. (b) A histogram showing the size distribution of oleate-capped ZnSe QDs. The particles size (diameter) is in the range of between 3.6 to 6.1 nm.

3.1.5 ODA-capped ZnSe QDs

Groeneveld et al. used a method of synthesis similar to the Hines and Guyot-Sionnest procedure, but with a different capping ligand.[61] They had octadecylamine on the surface of the QD instead of hexadecylamine. Figure 3.8 shows a ZnSe QD spectrum obtained from the sample collected using their method. However, it was difficult to make quality materials from their method, as pure particles could not be obtained due to difficulties in the purification process.

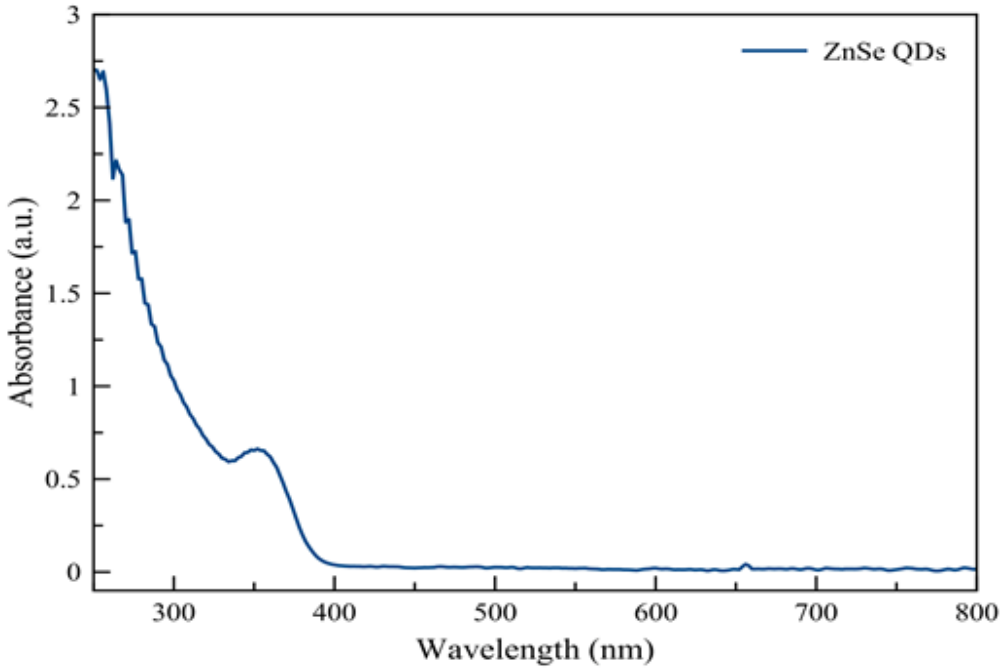

Figure 3.8. ODA-capped ZnSe QD absorbance spectrum.

3.1.6 Summary on ZnSe Synthesis

During the ZnSe synthesis using the various methods described above, there were difficulties in making quality materials. It was difficult to control the particle size and size distribution. However, Hines et al. and Shen et al. methods of preparing HDA-capped and oleate-capped QDs show some promising results with their absorbance spectra, TEM images, XRD patterns and their purification processes. Therefore, we proceeded to investigate cation exchange reactions with ZnSe QDs obtained using the Hines and Shen methods of synthesis as a starting material for Ag_2Se QDs.

3.2 Cation Exchange Reaction of ZnSe to Ag_2Se QDs.

3.2.1 Cation Exchange of HDA-capped ZnSe QDs to Ag_2Se

The attempt to make high quality ZnSe QDs, which will serve as the starting material for the exchange was challenging. Purification of ZnSe QDs to achieve clean particles, by getting rid of unreacted Zn and Se precursors in the sample, was difficult to achieve by the usual methods. The TEM image as shown for HDA-capped ZnSe QD shows that the particle sizes are not uniform. However, an exchange reaction was carried out with these ZnSe QDs to investigate the possibility of exchanging Zn for Ag using relatively cheap, nontoxic, available materials, and the cation exchange experiments were investigated at room temperature.

a. **b.**

Figure 3.9. (a) HDA-capped ZnSe QDs resuspended in hexane after purification and (b) a dark solution of Ag_2Se QDs after cation exchange.

The theoretical concept of hard and soft acids and bases (HSAB) introduced by Parr and Pearson is an idea that is useful in understanding the driving force for the cation exchange reaction.[49] In this experiment, Ag^+ is considered as the soft acid and Zn^{2+} is considered as the hard acid. The silver reagent is made up of oleylamine (OlAm), silver nitrate, acetonitrile, and toluene. OlAm and acetonitrile in the silver reagent act as hard bases, while the Se^{2-} bonded to the metal ion in the starting material (Zn^{2+}) serves as the softer base. Hard acids tend to bond strongly with hard bases, and likewise soft acids bond strongly to soft bases due to polarization of their electron clouds. OlAm and CH_3CN (hard bases) compete for Zn^{2+} ions (hard acid) in the reaction mixture, pushing out Se^{2-} ions (soft base) which proceed to bond strongly with Ag ions (soft acid). This concept contributed to the driving force for the reaction to occur. Ag_2Se QDs were produced as the target product with Zn^{2+} present in the reaction mixture. Unreacted precursors and Zn^{2+} were removed through purification procedure described in chapter 2 to obtain pure Ag_2Se QDs. Figure 3.9 (a) and (b) show a color difference comparing before and immediately (few seconds) after the Ag^+ ion reagent was introduced to the ZnSe QDs solution.

$$ZnSe + 2\,Ag^+ \longrightarrow Ag_2Se + Zn^{2+} \qquad (3.1)$$

Figure 3.10 shows an absorption spectrum of Ag_2Se QDs obtained from the exchange reaction. It is obvious that a new type of QDs has been formed, as the

typical absorbance peak for ZnSe is absent. The absorbance spectrum corresponds to that of Ag_2Se QDs.

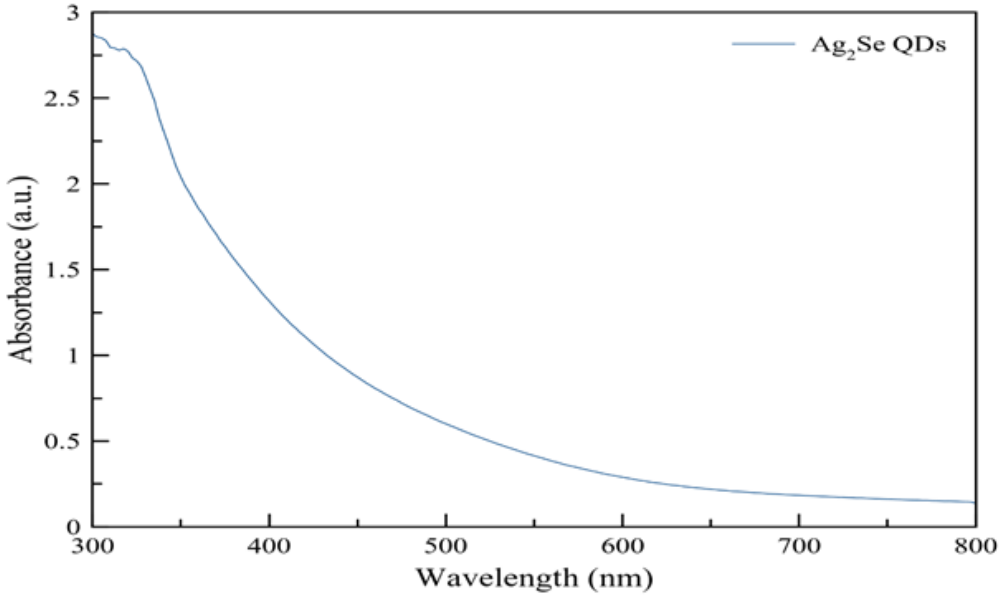

Figure 3.10. Ag_2Se QDs absorption spectrum prepared through cation exchange from HDA-capped ZnSe QDs.

The TEM image in Figure 3.11a shows there are particles in the exchanged mixture. However, the particle size observed before the exchange does not correspond to the size seen after the exchange reaction. There was an increase in size of the particles, which was analyzed to be 7.2 nm with standard deviation of 2.6 nm corresponding to the histogram in Figure 3.11b. An increase in the particle size when compared to the size of the starting material, which was 5.1 nm

with standard deviation of 1.5 nm was expected. A calculation of the volumes of the starting material (ZnSe) and the exchanged product (Ag_2Se) with respect to the number of their moles, formula weight and density was done as shown in equation 3.2 below. A theoretical increase of 32% in volume was calculated for the cation exchange from ZnSe QDs to Ag_2Se QDs. However, the increase in size observed in this work is approximately 73%. The difference in the estimated volume as to the theoretical volume of the QDs after exchange can be attributed to the difficulty of making high-quality ZnSe QDs (starting materials).

$$\frac{V_{(\mathrm{ZnSe})}(\mathrm{mL})}{1} \times \frac{D_{(\mathrm{ZnSe})}\ (\mathrm{g})}{1\ (\mathrm{mL})} \times \frac{1\ (\mathrm{mol})}{FW_{(\mathrm{ZnSe})}\ (\mathrm{g})} \times \frac{FW_{(\mathrm{Ag_2Se})}\ (\mathrm{g})}{1\ (\mathrm{mol})} \times \frac{1\ (\mathrm{mL})}{D_{(\mathrm{Ag_2Se})}\ (\mathrm{g})} = V_{(\mathrm{Ag_2Se})}\ (\mathrm{mL}) \tag{3.2}$$

where *D* is density (g/mL), *FW* is formula weight (g/mol), and *V* is volume (mL)

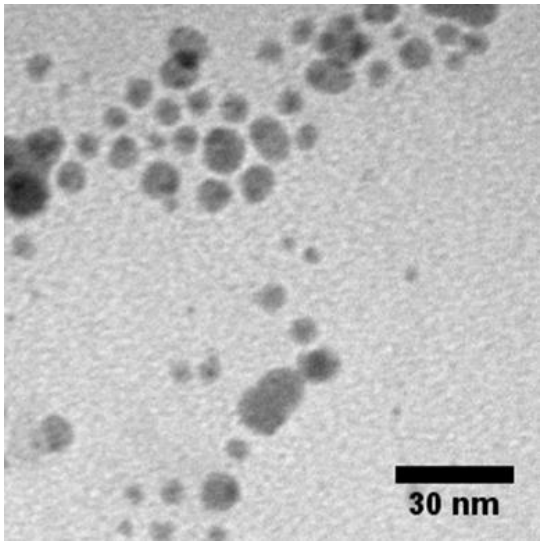

a.

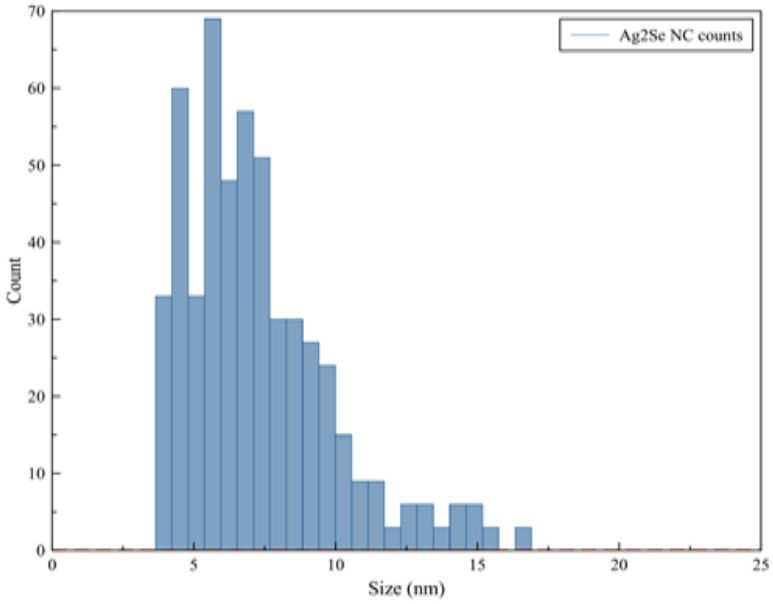

b.

Figure 3.11. (a) Exchanged Ag_2Se QDs TEM image showing increase the size of particles before the exchange. (b) Size distribution of exchanged Ag_2Se QDs.

To further understand the new product formed in the exchange reaction, PXRD measurement was made with the Ag_2Se QDs sample. Figure 3.12 shows a PXRD pattern that confirms the presence of cubic phase Ag_2Se QDs. The red bars in the figure relate to the known peak positions for cubic phase Ag_2Se QDs.[66]

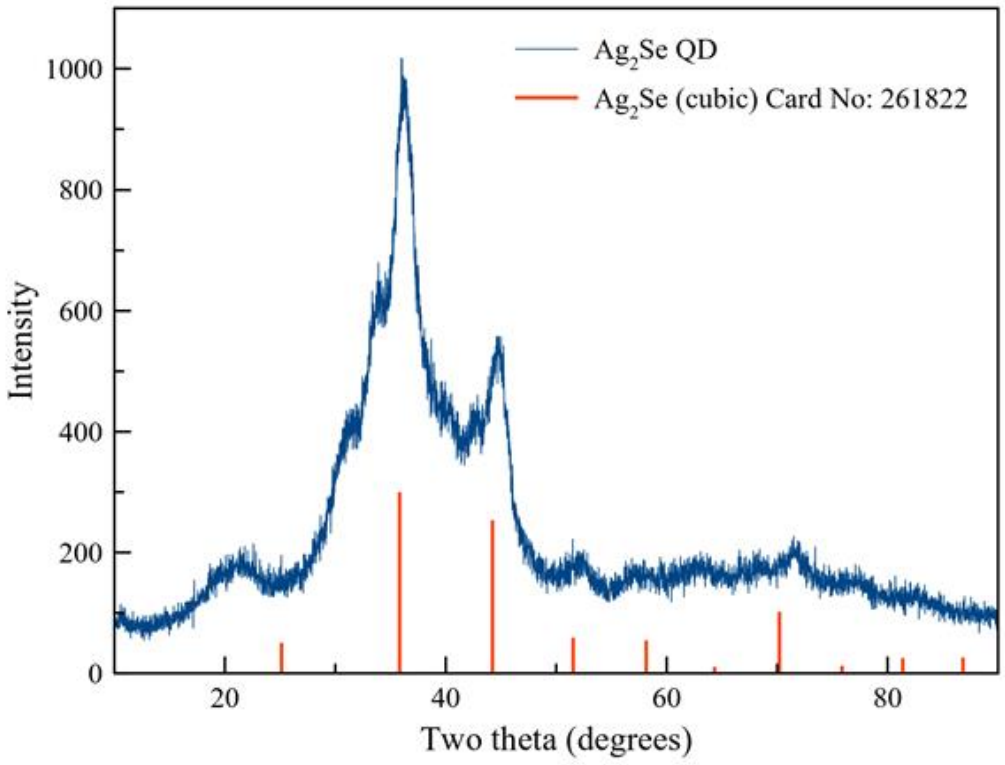

Figure 3.12. X-ray diffraction pattern of Ag-exchanged ZnSe QDs. The corresponding peaks show the presence of cubic Ag_2Se structured QDs.[66]

3.2.2 Oleate-capped ZnSe QDs Cation Exchange to Ag_2Se

Using the oleate-capped ZnSe QD as a starting material, a cation exchange of Zn^{2+} to Ag^{+} was also investigated. The absorption spectrum shown in Figure 3.13 confirms the exchange reaction occurred. However, there were difficulties synthesizing ZnSe QDs (starting material) with size control and uniform size distribution. The TEM image in Figure 3.14(a) also shows an increase in the size of the particles after exchange reaction. The size distribution was analyzed using

multiple TEM images obtained from Ag_2Se QDs sample. Mean particle size was determined to be 5.4 nm with a standard deviation of 1.0 nm. The histogram for the size distribution is shown in Figure 3.14(b). The histogram shows that the particles are not uniform in size. The increase in particle size can be explained due to the change in molar volume of Ag_2Se mentioned above.

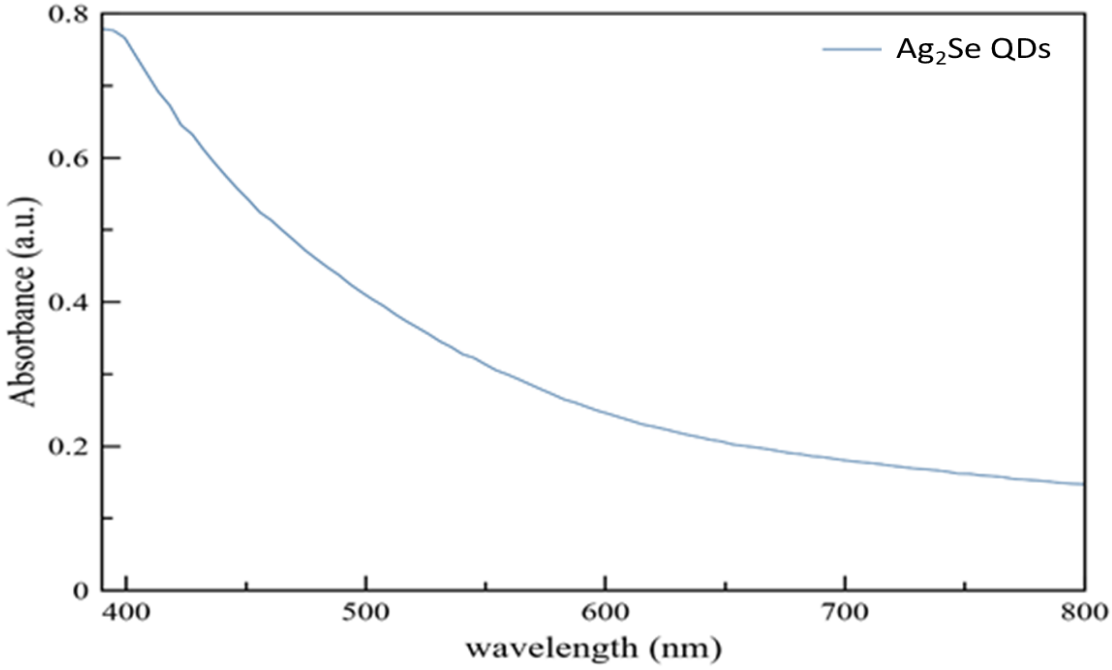

Figure 3.13. Visible absorption spectrum of Ag-exchanged ZnSe QDs. Absorbance peak observed on the ZnSe spectrum is not seen here, as Ag_2Se QDs absorb in the far infrared region.

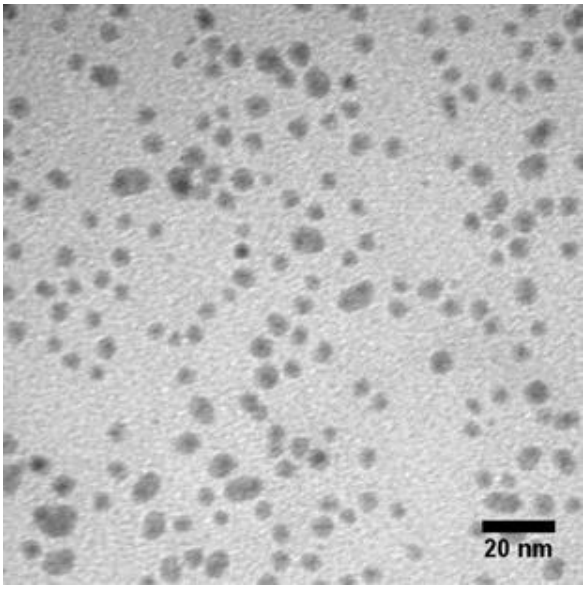

a.

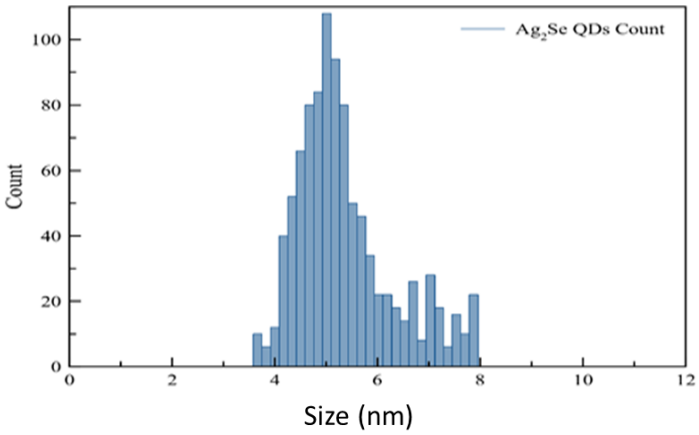

b.

Figure 3.14. (a) TEM image showing Ag_2Se QDs after the exchange reaction. Growth in the size of the exchanged particles compared to the starting material can be observed on this image. (b) Histogram of the Ag_2Se particle population showing the size distribution of the particles.

3.3 Comparison of cation exchange reaction rate using ZnSe and CdSe as starting materials.

A stopped-flow technique involving the rapid mixture of two or more solutions was used to measure the reaction kinetics for the cation exchange reactions. The reaction kinetics from Zn^{2+} and Cd^{2+} exchange to Ag^{+} were studied. CdSe QDs sample synthesized with Wu et al. method of synthesis,[29] and oleate-capped ZnSe QDs[62] method were used for this study.

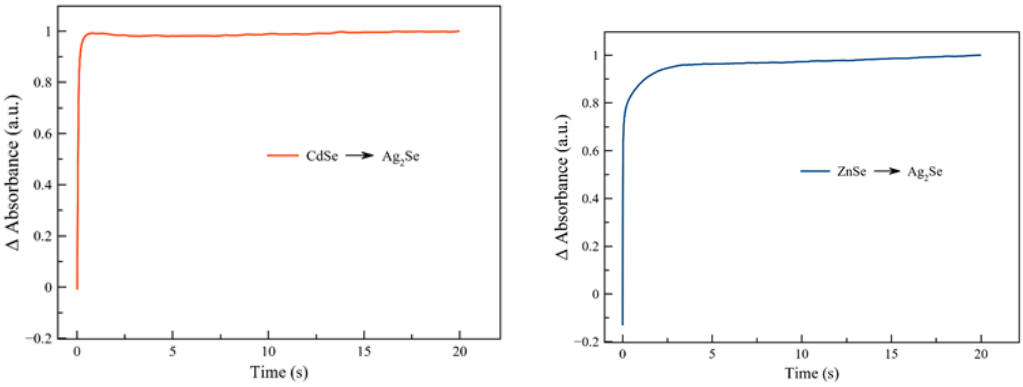

a. **b.**

Figure 3.15. (a) shows a stopped-flow kinetics curve of the Cd exchanged Ag_2Se QDs reaction, (b) stopped-flow kinetics curve of Zn exchanged Ag_2Se particles.

Figure 3.15 shows the normalized change in absorbance at 600 nm wavelength versus time during Ag^{+} exchange in (a) ZnSe and (b) CdSe QDs. The curves have been placed on the same graph in Figure 3.16 for detailed

comparison. The time axis in Figure 3.16(a) is linear, while that shown in 3.16(b) is plotted on a logarithmic scale. Figure 3.16(b) highlights details of the early stage of the exchange reaction and emphasizes the multi-phasic character of the reaction. This is particularly evident in the case of the ZnSe exchange, which shows a rapid initial change, followed by a leveling out around 0.1 s. This type of curve profile cannot be fit by a simple exponential, but instead must be fit to a curve with multiple rate constants.

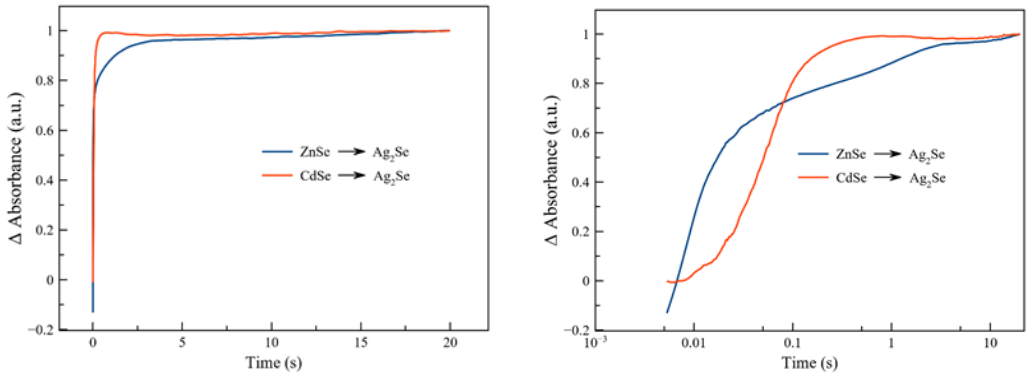

Figure 3.16. Comparison of the stopped-flow kinetics curve of both CdSe (red line) and ZnSe (blue line) as starting materials on the same scale. (a) Linear time scale. (b) Logarithmic time scale.

Fitting was done on the curves as shown in Figures 3.17 and Figure 3.18 in order to quantify the reaction rates for direct comparison using the mathematical

expression (3.3). This expression was found as a result of trying several different test functions to find a way to directly compare the relative values of the rate constants of various stages of the cation exchange reaction.

$$y = A * \{1 - \exp[-k_1(x)]\} + B * \{1 - \exp[-k_2(x)^{\beta}]\} + C * \{1 - \exp[-k_3(x)]\} + z \quad (3.3)$$

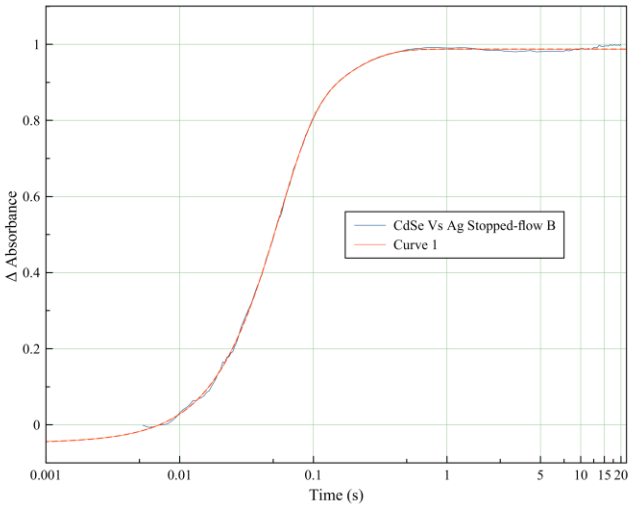

Figure 3.17. Stopped-flow kinetics curve fitting of Ag exchanged CdSe QDs. The fitting was done using equation 3.3 above.

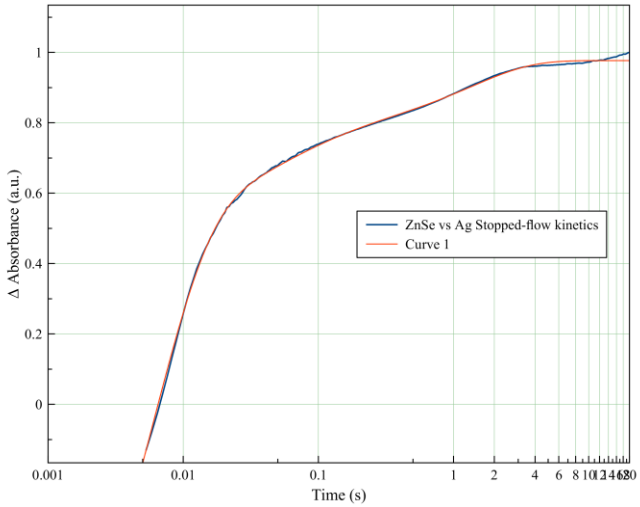

Figure 3.18. Ag exchanged ZnSe QDs stopped-flow curve fitting using equation 3.3. A best fit was achieved with three rate constant values (k_1 – k_3).

Use of this equation gave good fits to all the data collected on these samples. Table 3.1 shows the corresponding values of the fit parameters, which helps to better compare and understand the reaction kinetics.

Table 3.1. Fit results for the Ag exchange reaction kinetics

Starting Materials	k_1 (s^{-1})	k_2 (s^{-1})	k_3 (s^{-1})	**Beta**	***A***	***B***	***C***
CdSe	9.00 ± 3.00	110.0 ± 70.0	0	1.57	0.722	0.313	0
ZnSe	190 ± 20.0	7.00 ± 1.00	0.707	0.530	1.54	0.462	0.192

It was assumed that the exchange reaction in both systems started at the surface of the QDs corresponding to high reaction rate constant (k_1) observed, before further reactions in the inner core. Once the exchange reaction at the surface is complete, the exchange progresses to the inner core of the QDs, where metal ions have to move through the lattice in order to reach the inner core of the QDs. The movement of the metal ion slows down due to the difficulty to move through the lattice of the host material, therefore slowing down the reaction rate as observed with the later exchange rate. The slower steps of the reaction connote the rate constants k_2, k_3, depending on the stages of reactions involved to achieve a complete exchange.

An equivalent function (equation 3.3) was used to fit both curves of CdSe and ZnSe to obtain best fits. However, the value of C and k_3 is not important to get a good fit for the CdSe curve. The values of C and k_3 can be chosen over a wide range (with large standard deviation) for the CdSe curve and still have a good fit for the curve with the same values of k_1 and k_2. Therefore, both C and k_3 are set to zero (0) which show no effect on other variables and a good fit was achieved.

The large k_1 value of 1.9×10^2 s^{-1} for ZnSe corresponds to the faster kick start and later slow stage as confirmed with the k_2 value of 7.0 s^{-1}. The opposite was seen in CdSe with slower start corresponding to lower k_1 value of 9.0 s^{-1} and faster further stage reaction with a high k_2 value of 1.1×10^2 s^{-1} through the exchange reaction process. Slower rate of reaction observed later with lower k_2 value in the ZnSe compared to CdSe system can be attributed to the shorter length

(2.50 Å) and stronger Zn-Se bond as to longer Cd-Se bond length (2.65 Å).[68] Longer bonds give more room for Ag^+ ions to move easier through the CdSe lattice, whereas the shorter and stronger Zn-Se bond makes it hard for Ag^+ ion to change places with Zn^{2+}, due to less space for Ag^+ ions to move through the lattice. The bonds in the host QDs also need to be broken to allow formation of new bonds with incoming metal ions. A Zn-Se bond enthalpy of 170.7 ± 25.9 $kJmol^{-1}$ increases the energy required to break the Zn-Se bond compared with 127.6 ± 25.1 $kJmol^{-1}$ bond enthalpy[71] of a Cd-Se bond. The activation barrier associated with bond breaking can partially explain the slower k_2 value observed for ZnSe QDs.

One major goal of this work was to systematically compare reaction rates between ZnSe and CdSe QDs. We have shown some key differences between specific ZnSe and CdSe QD samples and commented on the implications of these differences. However, the difference in the kinetics of cation exchange reaction exploring ZnSe or CdSe as the starting material was not concluded in this work. This was due to the difficulty of making high quality ZnSe QDs compared to CdSe QDs. We were never able to exert adequate control over particle size and size distribution of the ZnSe QDs to enable direct comparison of an entire series of ZnSe QD samples with an analogous series of similar-sized CdSe QDs.

3.4.1 Summary

Our goal to develop a method for cation exchange reaction using environmentally friendly material (ZnSe) in place of Cd containing materials was achieved, but there is still a need to successfully make high quality ZnSe QDs to study the Zn system for a better comparison with the Cd system. While ZnSe QDs were prepared, and these QDs show rapid, room-temperature cation exchange with Ag^+, the particles did not exhibit the same narrow size distributions that are possible with CdSe QDs. Moreover, we could not deliberately control the particle sizes, nor could we reliably purify the particles in sufficiently large quantities to make them comparable to CdSe QDs as a starting material for cation exchange reactions. However, we were able to successfully carry out a cation exchange reaction from ZnSe to Ag_2Se, which was evident in the absorption spectra and PXRD patterns before and after the exchange reaction.

4 KINETIC STUDY OF CATION EXCHANGE REACTIONS IN CdSe QDS COATED WITH DIFFERENT CAPPING LIGANDS

The ligands on the surface of QDs play a role in the cation exchange reaction. Nonpolar solvents such as toluene coupled with the right ligands, can serve as a Lewis base that takes part in driving cation exchange reactions. A list of phosphine (R_3P) ligands were studied by Gui et al. to understand their activity in the cation exchange of Ag_2S to CdS.[67] Phosphine ligands, which are considered to be soft Lewis bases, took part in the exchange reaction by forming a stable ion-ligand complex with the Ag^+, which is a Lewis soft acid compared to Cd. This promotes the formation of CdS. Similarly, an exchange from CdSe to Ag_2Se was triggered by the presence of oleylamine, which is a Lewis hard base in the Ag ion reagent in the exchange reaction. The reaction promoted Ag_2Se and Cd-OlAm complex formation.

While Gui's work focused on the ability of the phosphine ligands to coordinate to the metal cations present in the solution, the capping ligands on QDs can also play a completely different role in regulating the cation exchange reaction. They can be thought of as "gate-keepers" to the QD surface. As Ag^+ cations present in solution approach the QD, they must penetrate the corona of ligand molecules and migrate to the surface before exchanging with a Cd^{2+} cation at the surface. Since the experiments described here are performed in non-polar solvents such as hexane and toluene, these solution-phase metal cations are almost certainly bound to ligands of their own. The steric interactions between these

solution-phase cation-ligand complexes and the cation-ligand complexes at the QD surface may slow the cation exchange reaction. It is not known whether these surface interactions are significant compared to other kinetic factors, such as the stepwise migration of the metal cations through the QD crystal lattice. Here we examine the impact of different surface ligands on the kinetics of the cation exchange reaction in CdSe QDs in an effort to learn whether surface interactions are sufficiently important to be a determinant of reaction rate.

The effect of different amine ligands on the rate of cation exchange was studied in this work. Amine capping ligands including oleylamine (OlAm), dodecylamine (DDA), hexadecylamine (HDA), and trioctylamine (TOA) were investigated. CdSe QDs were synthesized using the method reported by Wu et al. The same batch of CdSe QDs (0.25 mL per aliquot) was purified and treated with 0.050 mL of each of the amine ligands in separate tubes. This treatment allowed the amine ligands to replace the native ligands that were present after QD synthesis. HDA and DDA are saturated organic compounds, which allows their chains to pack tightly together. This characteristic favors strong van der Waals interactions and results in these compounds being solid at room temperature. In these experiments, these ligands were heated to their melting point to facilitate dissolving them to the CdSe QDs [toluene] solution.

Figure 4.1 shows an absorption spectrum of CdSe QDs before treatment with ligands. DART-MS measurements by Dr. Mengliang Zhang showed that the as-prepared CdSe QDs are coated primarily with HDA and tri-octylphosphine

oxide. The absorbance peak observed at 580 nm corresponds to the presence of CdSe QDs in the analyzed sample. The sharp absorbance peak indicates that the QDs have a narrow size distribution.

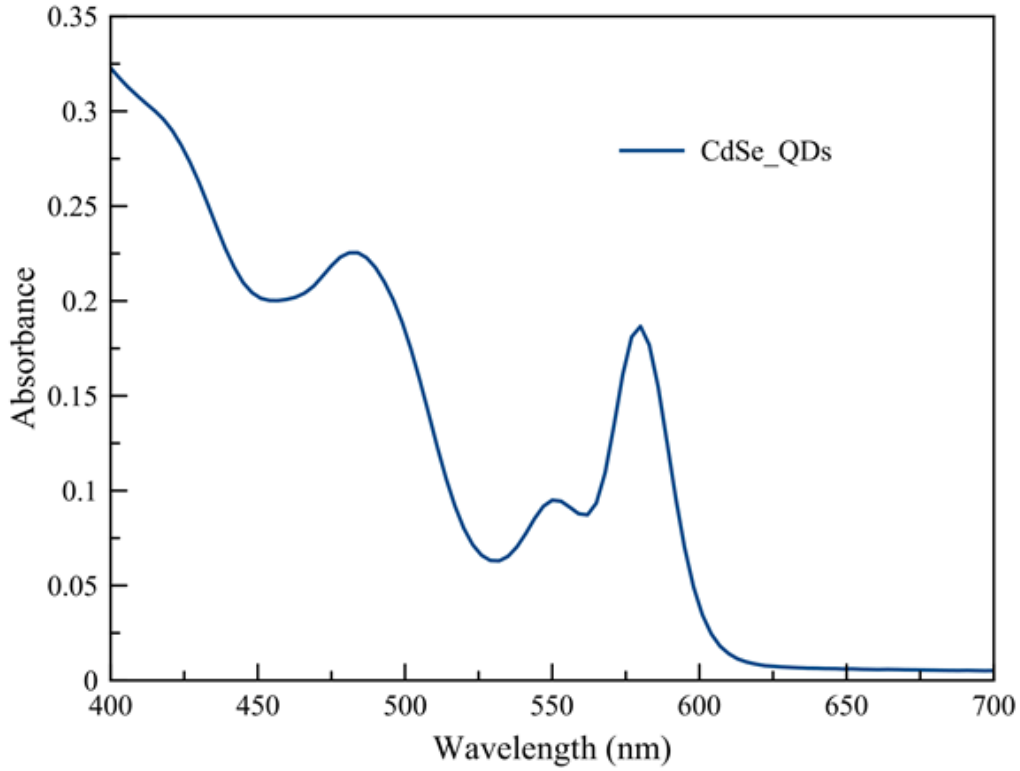

Figure 4.1. UV spectrum of the synthesized CdSe QDs before treatment with ligands.

The state of the ligand-exchanged CdSe QDs was investigated. UV absorption spectra show a blue shift of the lowest energy absorption peak following the introduction of amine ligands. The untreated CdSe QDs used in this experiment

had their lowest-energy absorbance peak at 580 nm. After the ligand treatment the absorbance peak of the ligand exchanged particles was observed according to the UV spectra to be at the range of 550 to 565 nm as shown in Figure 4.2 below. This blue shift could be due to electronic effects of the ligands, or, more likely, to etching of the QD surface that led to a slight shrinkage of the QD particle size.

The ligand treatment shrinks the particle to a size smaller than the untreated CdSe particles. The size in diameter of the particles were calculated using the function developed by Yu et al.[63]

$$D(\text{nm}) = (1.6122 \times 10^{-9})\lambda_a^4 - (2.6575 \times 10^{-6})\lambda_a^3 + (1.6242 \times 10^{-3})\lambda_a^2 - (0.4277)\lambda_a + 41.57 \quad (4.1)$$

D is the diameter of the particle and λ_a is the wavelength of the absorbance peak with the highest wavelength.

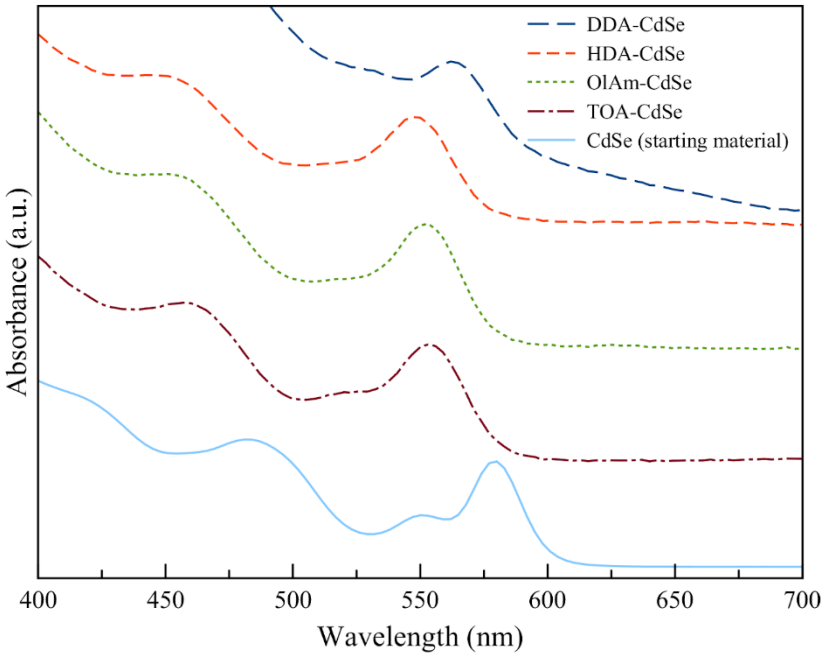

Figure 4.2. Absorbance spectra of CdSe QDs before and after ligand exchange.

The untreated CdSe particle has its absorbance peak at 580 nm as seen in Figure 4.1. Particle size was calculated to be 3.8 nm. Figure 4.3, 4.6, 4.8, and 4.10 show the absorbance peak of particles treated with OlAm, HDA, DDA, and TOA respectively. The absorbance wavelength and calculated size corresponding to the ligands are listed on Table 4.1.

Table 4.1. Calculated size and wavelength corresponding to the ligands on the surface of the QD.

Ligands	Wavelength (nm)	Diameter (nm)
HDA	550	3.0
DDA	562	3.3
OlAm	553	3.1
TOA	553	3.1

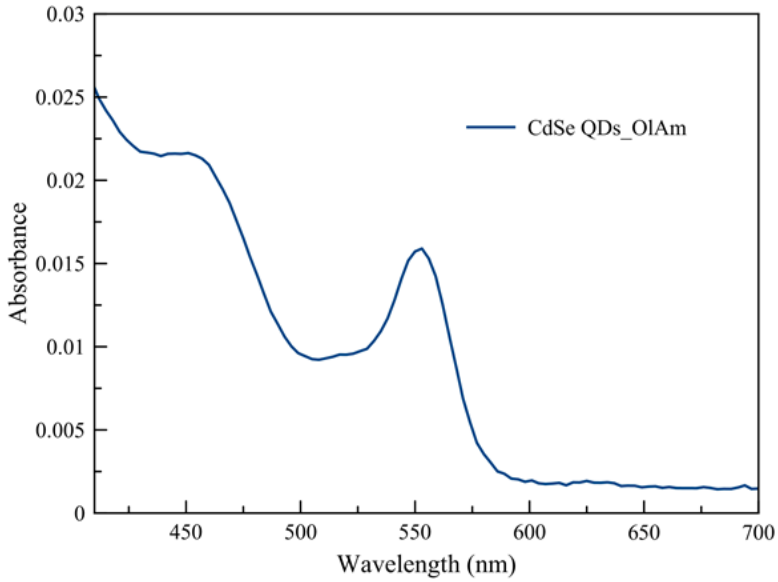

Figure 4.3. Oleylamine treated CdSe QDs UV absorption spectrum.

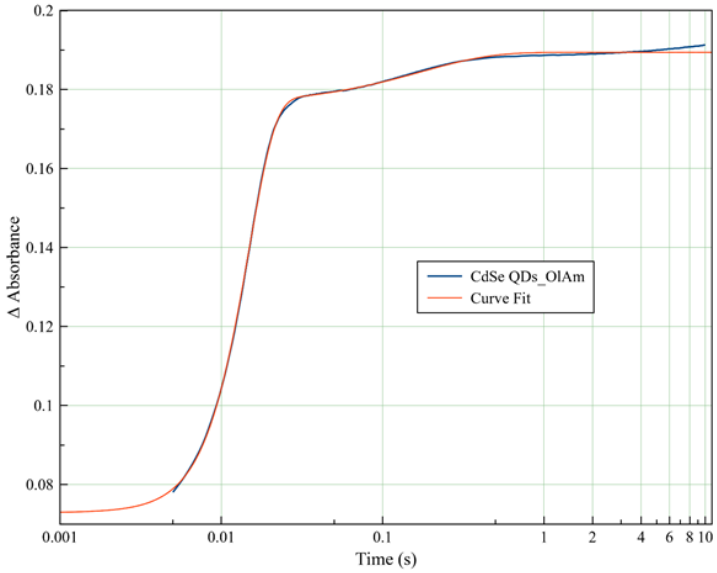

Figure 4.4. Stopped-flow kinetics curve for oleylamine-treated CdSe QDs, showing the experimental curve (blue line) and the curve fit (red line).

The stopped-flow kinetics experiment curve is a real time measurement of change in absorbance over time, measured at a wavelength of 400 nm, as the cation exchange reaction took place in the stopped-flow instrument. The kinetics curves show an obvious difference in the rate of reaction depending on the ligands on the surface of the QDs as shown in Figure 4.5. However, after trying several different functions, a mathematical expression (equation 4.2) with respect to k (rate constant) values was developed to better understand the rate at which the exchange reaction occurred. This gives a way to directly compare the relative values of the rate constants of the various stages of the reaction.

$$y = A * \{1 - \exp[-k_1(x)^{\beta}]\} + B * \{1 - \exp[-k_2(x)]\} + z \qquad (4.2)$$

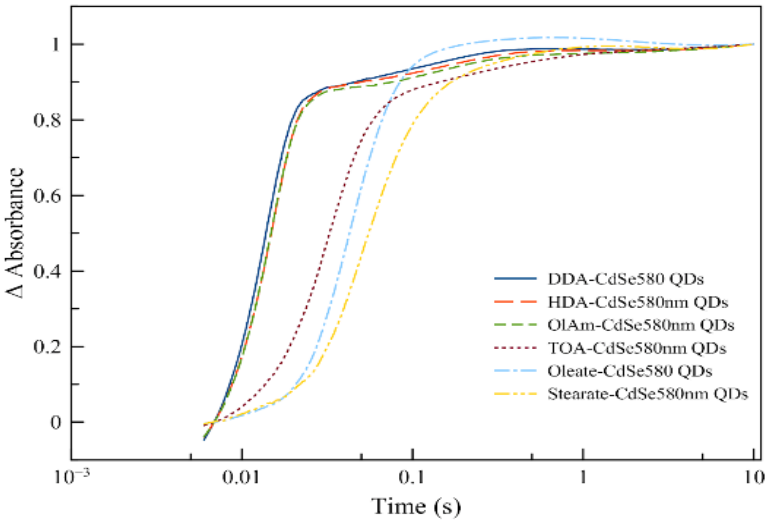

a.

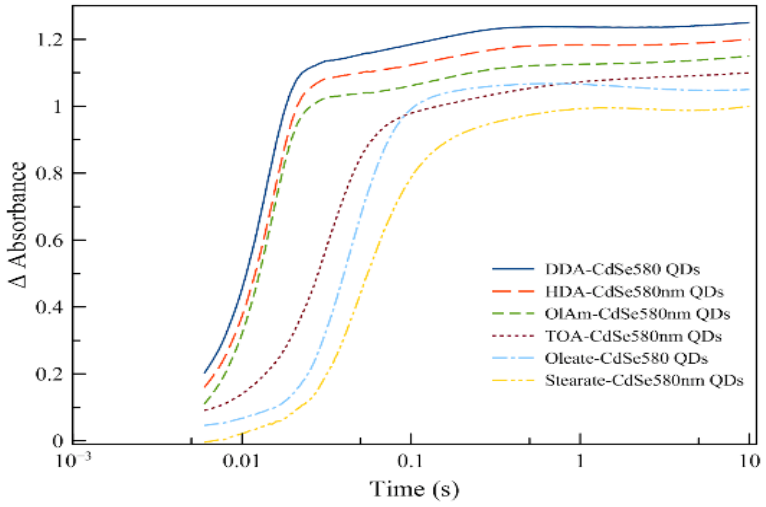

b.

Figure 4.5. (a) Kinetic curves obtained from the cation exchange reaction of ligand exchanged CdSe QDs and (b) is showing the kinetic curves being spaced out.

The exchange reactions involved in this experiment were run under pseudo-first order conditions. To achieve pseudo-first order conditions, the concentration of the metal ion (in this case Ag^{+} ion) was ten times the concentration of the Cd^{2+} ions contained in the QDs.

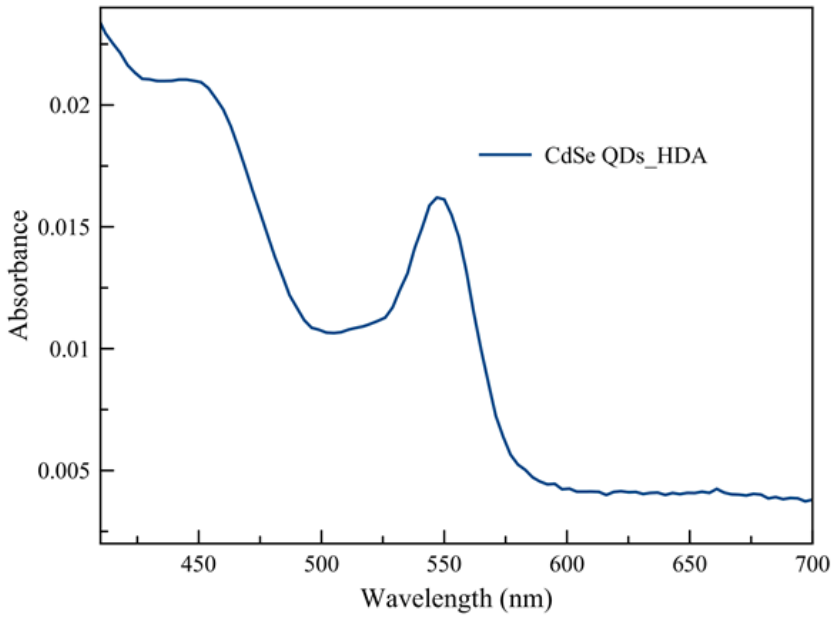

Figure 4.6. UV absorption spectrum for hexadecylamine treated CdSe QDs

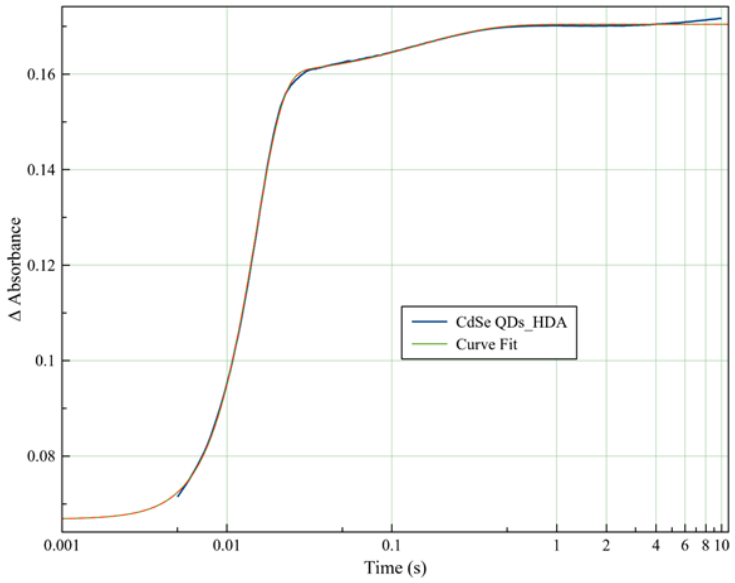

Figure 4.7. Stopped-flow kinetics curve for hexadecylamine treated CdSe, showing the experimental curve (blue line) and the curve fit (red line).

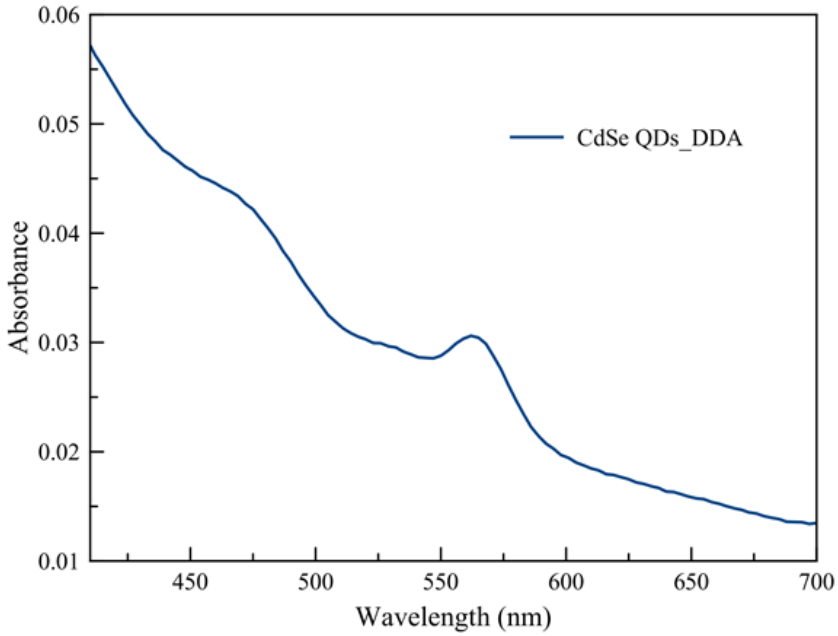

Figure 4.8. Dodecylamine treated CdSe QDs UV absorption spectrum.

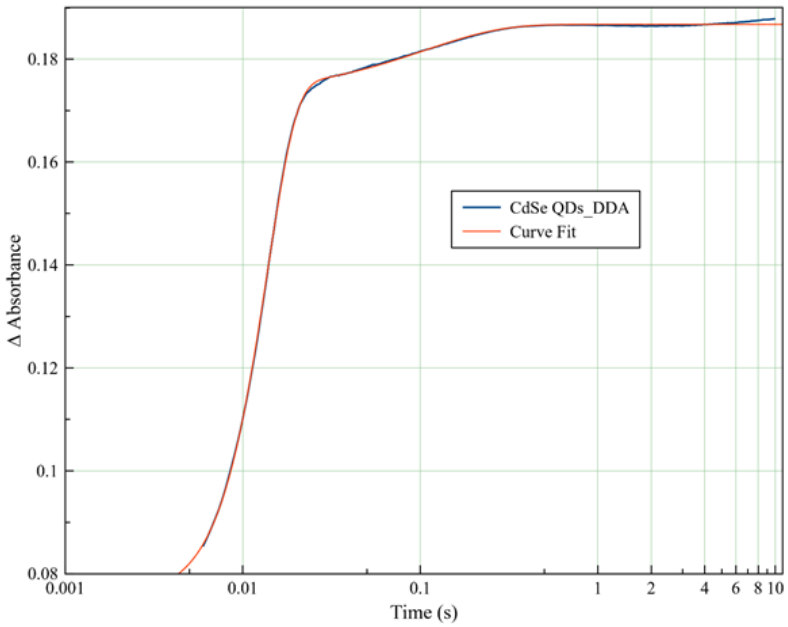

Figure 4.9. Stopped-flow kinetics curve for dodecylamine treated CdSe.

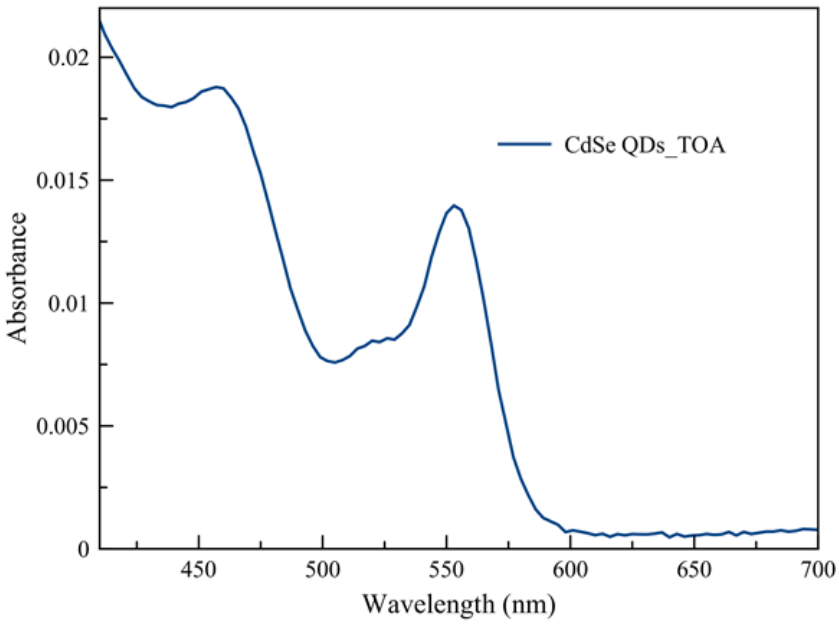

Figure 4.10. Trioctylamine treated CdSe QDs absorbance spectrum.

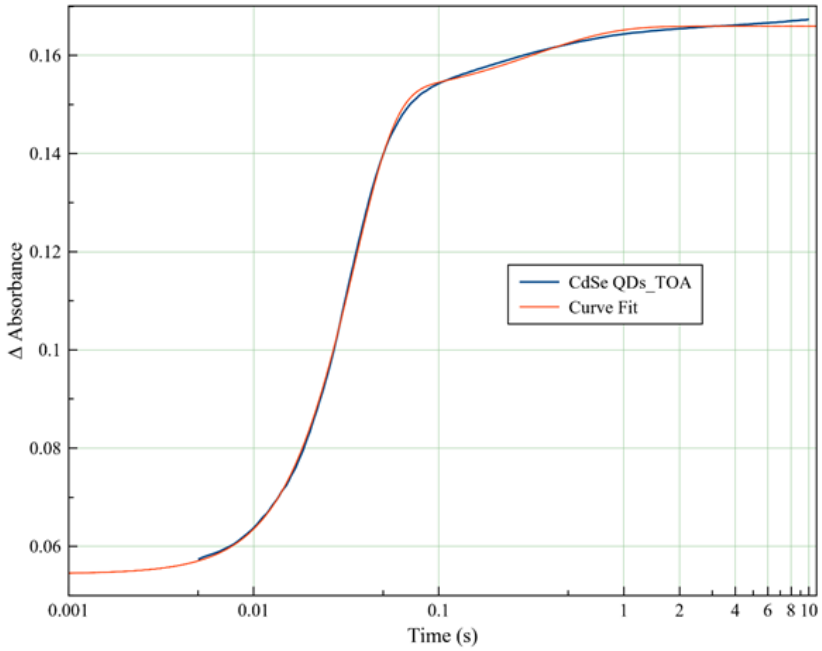

Figure 4.11. Stopped-flow kinetics curve for trioctylamine treated CdSe, showing the experimental curve (blue line) and the curve fit (red line).

The information in Table 4.2 shows the kinetic fit data from the CdSe QDs treated with the various ligands. The measured rate constants vary for ligands depending on their chain length, saturation, and steric effects. The cation exchange reaction involves a metal ion (Ag^{+}) that diffuses through a solvent (toluene) to replace the metal (Cd^{2+}) in the QD. How quickly the metal ions move in the solvent towards replacing the Cd^{2+} by coming in contact with the QDs depends on the viscosity of the reaction environment and the size of the reacting species. The effective overall size of the QDs also depends on the chain length of the ligands on the surface of the particles since these ligand chains extend outward into the solution. QDs with long chain ligands on the surface have a higher effective

[QD+ligand] radius compared to particles with short chain ligands. Examples include dodecylamine (±1.39 nm) with a shorter carbon chain (C12) compared to hexadecylamine (±1.89 nm) with longer carbon chain (C16). Therefore, the contribution of the diffusion rate and the length of the ligands towards the reaction rate in cation exchange processes observed was estimated using the series of equations discussed below.

Table 4.2. Kinetics rate constants and beta values of different CdSe quantum base on the amine ligands attached to the surface.

Amines	k_1 (s^{-1})	***A***	**%A**	k_2 (s^{-1})	***B***	**%B**	**Beta**
Dodecylamine	110000 ± 20000	1.0	88	9.4	0.14	12	2.7
Oleylamine	90000 ± 20000	0.98	88	5.8	0.13	12	2.7
Hexadecylamine	70000 ± 16000	0.99	89	6.3	0.12	11	2.6
Trioctylamine	580 ± 20	0.89	86	3.0	0.14	14	1.9

Considering the [QD+ligand] radius, it is possible to estimate the diffusion-limited rate constant that describes the rate of collisions between metal cations and the outer ligand surface. The diffusion-limited rate constant,[51] which relates to the contact between two reactants that leads to a reaction, can be expressed as

$$k_D = 4\pi\ (D_A + D_B)\beta \tag{4.3}$$

In equation 4.3 above, k_D is a diffusion-limited rate constant, beta (*β*) is equal to *R* ($r_A + r_B$) for uncharged reactants which is the critical radius where r_A and r_B are the radii of reactants A and B, while D_A and D_B are diffusion coefficients of reactants A and B, respectively. The diffusion coefficient related to viscosity can be expressed by Stokes-Einstein equation[51]

$$\mathrm{D} = \frac{k_b T}{6\pi\eta r} \tag{4.4}$$

where *D* is the diffusion coefficient, k_b is Boltzmann's constant, *T* is temperature in kelvins, *ŋ* is viscosity, and *r* is the radius of a spherical particle.

The relationship between diffusion coefficient and radius of a spherical particle can be expressed with respect to the QDs and metal ion as

$$D_{QD} \propto \frac{1}{r_{QD}} \tag{4.5}$$

$$D_{M^+} \propto \frac{1}{r_{M^+}}, \tag{4.6}$$

where D_{QD} and D_{M^+} are QD and metal ion diffusion coefficients, respectively, and r_{QD} and r_{M^+} are QD and metal ion radii, respectively.

The diffusion coefficient is dependent on the radius of the reactants, and the diffusion-limited rate constant is dependent on the diffusion coefficient, as expressed in equation 16. The metal ion involved in the exchange reaction is assumed to have a constant radius, much smaller than the QD+ligand radius. In contrast, the QDs have radii which can be dependent on the chain-length of the ligands on its surface.

The trend seen with the amines in Table 4.2 shows that DDA-capped QDs with short carbon chain have the highest rate constant k_1 (1.1×10^5 s^{-1}), which implies a faster exchange reaction. The reaction rate becomes slower ($k_1 = 7.0 \times 10^4$ s^{-1}) with the increased chain length of HDA. Since k_1 represents the fastest rate constant observed in the system, it seems likely that this represents the exchange of cations in the outermost surface layer of the QD, and this process is most likely to be strongly influenced by the metal cation/QD collision rate.

HDA and DDA are saturated organic molecules with the same chain packing density and functional group, but different chain length. The reaction rate was affected by the alkyl chain length, with the longer HDA chain leading to slower cation exchange reaction given that the effective overall size of the particles capped with HDA ligands is higher than that of the DDA-capped particles.

Therefore, the diffusion-limited rate constant of DDA-capped QDs is higher than that of HDA-capped QDs according to the equations described above.

In order to investigate the rate difference observed with HDA and DDA using the diffusion-limited rate constant k_D, the equations above were used to calculate the diffusion-limited rate constant of both cation exchange reactions of HDA-capped and DDA-capped CdSe QDs with the Ag^+ metal ion. The radius of the metal ion and the QDs were evaluated considering the particular ligand attached to them. Oleylamine bonded to Ag^+ ion was part of overall radius of the metal ion, as it was prepared with oleylamine present in the solution. The radii of the QDs were evaluated giving account for the ligands attached to the surface. The approximate length of the ligands on both the QDs and metal ion were evaluated using the C-C single and double bond lengths.

Using bond length: C-C = 0.154 nm, C=C = 0.133 nm and bond angle of 109.5^o.[69] the carbon chain in an organic molecule can be modeled as a series of triangles when written in its shorthand form depending on the length as shown in Figure 4.12 below. The base of two right-angle triangles which is the distance between two carbon atoms as shown below was calculated using trigonometry to be 0.252 nm.

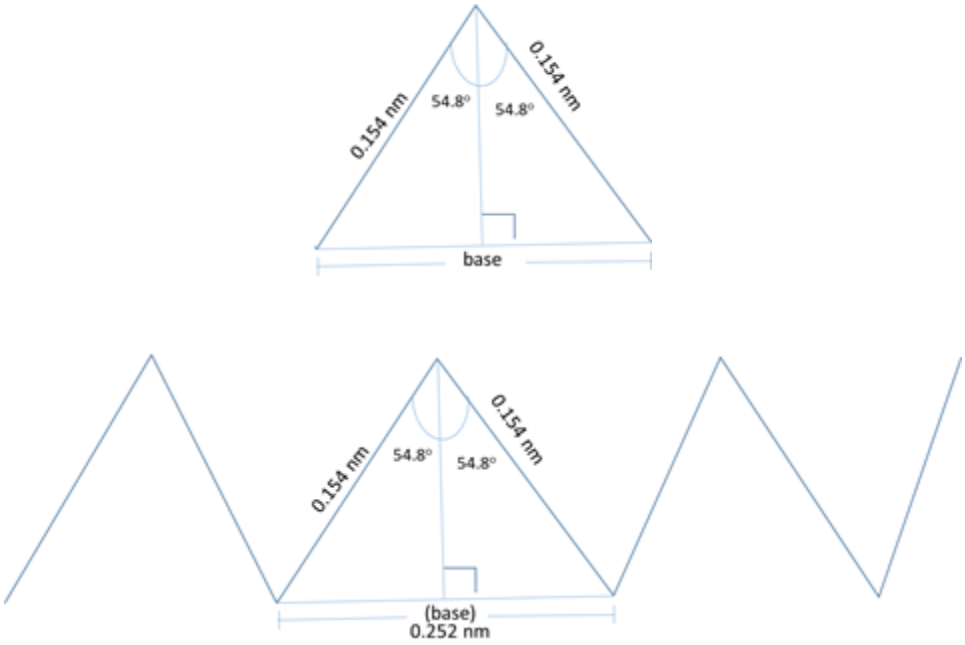

Figure 4.12. Typical shorthand structure of an alkane chain.

The length of the ligands was estimated summing up the distance between the carbon atoms in the organic molecules.

The following are estimated length of ligands:

Oleylamine (C18) = 2.15 nm

Dodecylamine (C12) = 1.39 nm

Hexadecylamine (C16) = 1.89 nm

The Ag^+ ion and CdSe QD core used in this experiment have a radius of 0.115 nm and 1.90 nm, respectively. Therefore, the overall effective radius of the metal ion and QD are

Ag^+–OlAm, = 2.27 nm

DDA-capped CdSe, = 3.29 nm

HDA-capped CdSe, = 3.81 nm.

Diffusion coefficient,

Boltzmann constant $k_b = 1.381 \times 10^{-23}$ m^2 kg s^{-2} K^{-1}

Temperature, T = 296 K

Viscosity of toluene, = 5.75×10^{-4} kg m^{-1} s^{-1}

π = 3.1416

$$D_{Ag^+} = \frac{1.381 \times 10^{-23} \times 296}{6 \times 3.1416 \times 2.26 \times 10^{-9} \times 5.75 \times 10^{-4}}$$

$$D_{Ag^+} = 1.67 \times 10^{-10}\ \mathrm{m^2 s^{-1}}$$

$$D_{QD-DDA} = \frac{1.381 \times 10^{-23} \times 296}{6 \times 3.1416 \times 3.29 \times 10^{-9} \times 5.75 \times 10^{-4}}$$

$$D_{QD-DDA} = 1.15 \times 10^{-10}\ \mathrm{m^2 s^{-1}}$$

$$D_{QD-HDA} = \frac{1.381 \times 10^{-23} \times 296}{6 \times 3.1416 \times 3.81 \times 10^{-9} \times 5.75 \times 10^{-4}}$$

$$D_{QD-HDA} = 9.90 \times 10^{-11}\ \mathrm{m^2 s^{-1}}$$

Relative diffusion-limited rate constants for the cation exchange reaction of DDA-capped and HDA-capped QDs are then calculated in terms of β, which is assumed approximately constant to be

$$k_D = 4\pi\ (D_{Ag+} + D_{DDA})\beta \qquad (4.7)$$

k_D, for DDA-capped QD = $4\pi\ (1.67 \times 10^{-10} + 1.15 \times 10^{-10})$

$= 3.54 \times 10^{-9}\ \mathrm{m^2 s^{-1}}$

k_D, for HDA-capped QD = $4\pi\ (1.67 \times 10^{-10} + 9.90 \times 10^{-11})$

$= 3.34 \times 10^{-9}\ \mathrm{m^2 s^{-1}}$

This analysis shows that the rate difference predicted from the diffusion-limited rate constants of the HDA- and DDA-capped QDs is only 6%. However, the rate difference observed with the rate constant k_1 from the kinetic curve is 36%. This difference can be accounted for by other effects such as the length of the ligands as shown in Figure 4.13, which could affect how fast the metal ion reaches the surface of the QD core from the outer surface of the ligand corona. The

expected ratio of rates caused by the chain length of the ligands (HDA C16 and DDA C12) was estimated to be 33%.

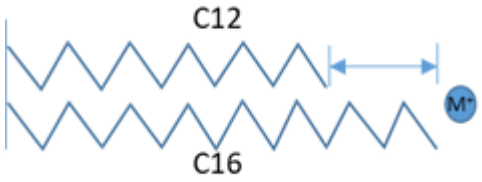

Figure 4.13. DDA and HDA chain length difference.

Thus, we conclude that the dominant effect of the ligands on the rate is to slow the migration of the metal cation to the surface from the ligand corona surface.

OlAm is a primary alkylamine with even longer chain length than HDA (C18 vs. C16). However, OlAm-capped QDs did not exhibit slower kinetics than HDA-capped QDs. Rather, they were faster, with rate constant (k_1) of 9.0×10^4 s^{-1} than the HDA-capped QDs with k_1 value of 7.0×10^4 s^{-1}. This rate difference observed with OlAm and HDA can be understood on the basis of steric effects. The movement of metal ion towards the QDs for collision, which leads to the exchange reaction can be hindered by the HDA ligand environment. HDA is a saturated organic molecule with its chains packed tightly together. This feature favors van der Waals interactions causing the molecule to be solid at room temperature. Therefore, HDA creates a ligand environment with an increased chain packing density on the surface of the QDs. However, OlAm on the other hand is an unsaturated organic molecule with a double bond at the center of the molecule,

and the double bond opposes chains packing tightly together. This characteristic creates a more disordered ligand environment with a decreased chain packing density on the surface of the QDs. The decreased density allows faster migration of the metal ion to the surface of the QDs, therefore, causing the reaction to be initiated more quickly.

An over 100 times slower rate of reaction with rate constant (k_1) value of 5.8 × 10^2 s^{-1} was observed with trioctylamine compared to other amines studied, and this can be attributed to the structure of the organic compound. Trioctylamine is a tertiary amine with three carbon chains attached to central atom (nitrogen) causing an increase in steric hindrance. Yu et al. reported that capping agents with branched structures protect the surface of the QDs better as compared to straight-chain ligands.[70] The hindered collision between the two reactants slows the actual rate of chemical reaction. A higher steric requirement of the reactant is expected to lead to a slow rate of reaction.

The effect of carboxylate ligands attached to the surface of the QDs on the rate of cation exchange was also studied in this thesis. Carboxylate ligands investigated include oleate and stearate to understand their contribution to the rate of cation exchange reaction. These ligands reported in this work show about five times difference in their rate of reaction as shown on Table 4.3. Stearic and oleic acids both have C18 chain length. Stearic acid is a saturated organic molecule, which allows its chains to pack tightly together with strong van der Waals interactions that result in stearic acid being solid at room temperature. There was

need to melt the stearic acid to its melting point to facilitate dissolution in CdSe QDs solution. Oleic on the other hand, is an unsaturated organic molecule with a double bond at the middle carbon results in disorder compared to saturated stearic acid.

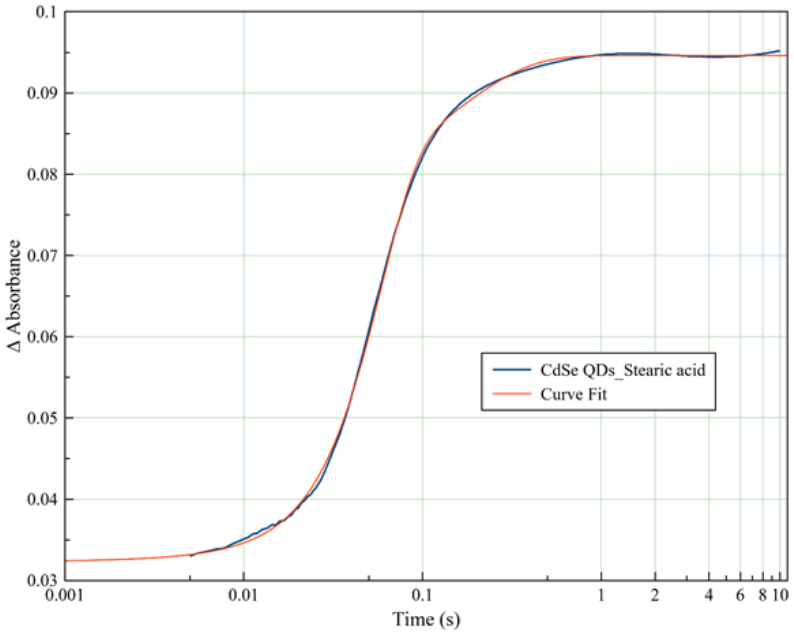

Figure 4.14. Stopped-flow kinetics curve for stearic acid treated CdSe, showing the experimental curve (blue line) and the curve fit (red line).

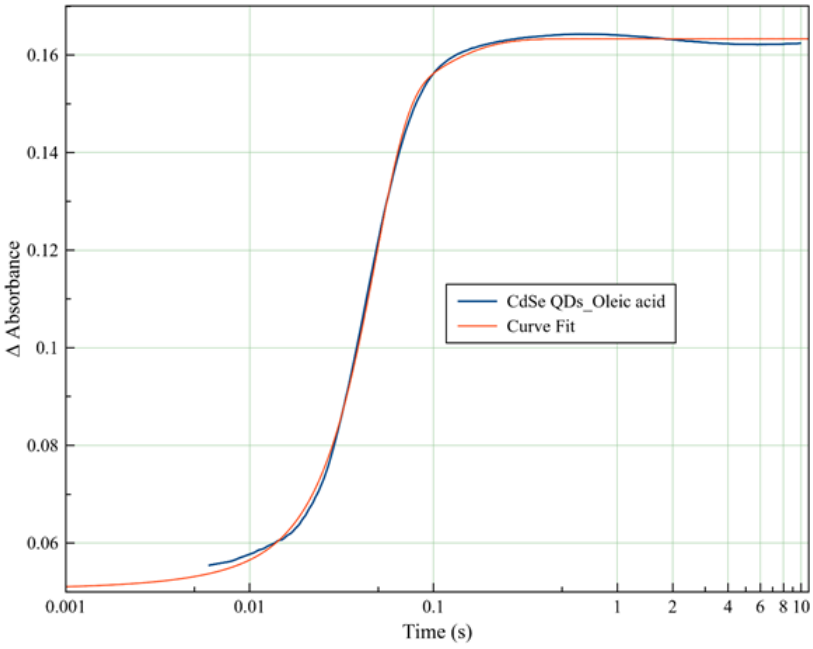

Figure 4.15. Stopped-flow kinetics showing oleic acid treated CdSe QDs curve.

Table 4.3. Kinetics rate constants and beta values of different CdSe quantum base on the carboxylate ligands attached to the surface.

Carboxylates	k_1 (s^{-1})	**A**	**%A**	k_2 (s^{-1})	**B**	**%B**	**Beta**
Oleate	1800 ± 150	0.76	72	15	0.29	28	2.5
Stearate	380 ± 60	0.70	69	6.9	0.32	31	2.1

The recorded difference in the rate of cation exchange reaction is dependent on the steric hindrance created by these capping ligands on the surface of the QDs. Stearic acid forms an increased chain dense ligand environment on the surface of the QDs. This leads to a more hindered migration of the metal ion to collide with the QDs. Therefore, such hindrance in migration results in a slow rate of chemical reaction observed with a k_1 value of 3.8×10^2 s^{-1}. The reaction process is faster for oleate-capped QDs with a resulting k_1 value of 1.8×10^3 s^{-1} owing to the reduced hindrance of metal ion migration towards collision with the QDs in the reaction solution.

A good comparison of carboxylate with amines are oleate and oleylamine respectively. The rate constant (k_1) of 1.8×10^3 s^{-1} relating to cation exchange reaction of oleate-capped CdSe QDs was observed to be approximately 42 times slower than oleylamine capped CdSe QDs with rate constant (k_1) of 9.0×10^4 s^{-1}. Both ligands are unsaturated organic molecules with similar carbon-chain-length (C18), but the only difference in their structure is the terminal functional group. The ligands were introduced to the CdSe QDs using similar parameters such as QDs to ligands ratio of 5 to 1. Such a significant difference in the rate of the exchange can be attributed to the different functional groups of the ligands, which is the primary bond site to the surface of the QDs and the ligands binding ability.

Oleate forms an ionic bond with the QDs giving rise to a strong ionic interaction at the surface of the QDs. Such interaction can increase the bond strength which minimizes disruption of the ligand at the surface of the crystals. This

can lead to an increase in the probability of having a very dense ligand population at the QD surface making it difficult (increased steric effect) for metal ion migration towards collision with the particle surface. The difficulty of ion migration leads to the slower rate of reaction observed with oleate-capped QDs. OlAm on the other hand forms relatively weaker bond on the surface of the QDs when compared to oleate, which makes the ligands loosely bonded to the particles. The QD-OlAm bonds are easier to disrupt than the QD-oleate bonds and may result in a less dense ligand population at the surface of the QDs. The less dense ligand environment gives room for easier metal ion migration towards the QD surface leading to a faster rate of cation exchange reaction.

5 Conclusion

Cation exchange reactions have been heavily studied with CdSe QDs as starting materials to synthesize Ag_2Se QDs. However, the study of ZnSe QDs as a starting material for cation exchange reactions is rare. In this thesis, zinc selenide QDs were synthesized through different procedures to achieve a high-quality starting material. A purification method for the ZnSe was described; however, after exploring different purification procedures, a perfect material devoid of unreacted precursors was not achieved.

The cation exchange reaction was successfully performed with exchange of Zn^{2+} for Ag^{+} ions, and a purification procedure for the exchanged particles was described. The QDs were analyzed before and after exchange reaction via Vis/NIR absorbance. ZnSe QDs sample has the characteristic peak present in its spectrum. While exchanged samples had the ZnSe QDs peak disappeared at every exchange done, giving absorbance spectra that correspond to Ag_2Se QDs. The PXRD pattern of before and after exchange samples show the presence of ZnSe crystals and Ag_2Se crystals respectively. TEM images show the particle sizes of ZnSe and Ag_2Se QDs with a significant increase in the sizes of Ag_2Se particles. A possible cause of the size increase was mentioned.

A comparison study was done to understand the kinetics of using ZnSe as to known system of CdSe as the starting material for cation exchange reaction synthesis of Ag_2Se. Real-time exchange rate was measured using a stopped-flow

kinetic instrument. There were variations in the rate of cation exchange in both systems and a mathematical equation was developed to understand and better explain how the reactions progressed.

The consequences of the type of ligand bonded to the surface of CdSe QDs on the rate of cation exchange with Ag^+ ion was investigated. Cadmium selenide was synthesized, purified and further treated with amines and carboxylates. The reaction rate with respect to the ligand attached to the QDs was measured on a stopped-flow kinetic instrument. The rate constant (*k*) values for the reactions were deduced with an equation developed to fit the kinetic curves. Significantly different rates of chemical reaction were observed with each ligand studied.

Further investigations are needed. A more reliable method could be developed for the synthesis of high-quality ZnSe QDs with better size control, narrow size distribution and scalability. Although much has been done to develop a suitable purification method for synthesized ZnSe QDs, it was difficult to get all the particles out of solution. A Comparison of the ZnSe and CdSe systems can be further investigated for exchange with other metal ions, to understand whether the incoming metal ion influences the rate of reaction in both systems.

The bond strength of the ligands bonded to the surface of the QDs and the bonding influence on the reaction rates could be explored. The ratio of QDs to ligand used for post-ligand treatment could be varied to investigate the effect on the reaction rate.

REFERENCES

1. Shan J., Yanxi H., Zhanjun Gu, Lei Liu, Hai-Chen Wu Application of Quantum Dots in Biological Imaging," *Journal of Nanomaterials* **2011,** *2011*, 1-13.
2. Hyun, B.; Chen; Rey, D. A.; Wise, F. W.; Batt, C. A. Near-Infrared Fluorescence Imaging with Water-Soluble Lead Salt Quantum Dots. *Journal of Physical Chemistry B* **2007,** *111*, 5726-5730.
3. L. M. Nikolenko, V. F. Razumov, "Colloid quantum dots in solar cells", *Usp. Khim.*, *Russian Chemical Reviews* **2013,** 82, 429–448.
4. Kamat, P. V. Meeting the Clean Energy Demand: Nanostructure Architectures for Solar Energy Conversion. *Journal of Physical Chemistry C* **2007,** *111*, 2834-2860.
5. Frecker, T.; Bailey, D.; McBride, J.R.; Arzeta-Ferrer, X.; Rosenthal, S. J.; Review—Quantum Dots and Their Application in Lighting, Displays, and Biology *Journal of Solid State Science and Technology* **2016,** *5*, 3019-3031.
6. Jamie, C.; Henry S. L. QLED TV: Samsung's panel technology explained. *https://www.techradar.com/news/samsung-qled-samsungs-latest-television-acronym-explained* (accessed Sept 5, 2019).
7. S. B. Brichkin; V. F. Razumov Colloidal quantum dots: synthesis, properties and applications. *Russian Chemical Reviews*, **2016,** 85, 1297-1312.
8. Brus, L. E. Electron–electron and electron-hole interactions in small semiconductor crystallites: The size dependence of the lowest excited electronic state. Journal of Chemical Physcis **1984,** 80, 4403-4409.
9. D. Boer and P.J. Mulders *Advanced Quantum Mechanics;* Pearson Education: 2003; pp 159-162.

10. Bera, D.; Qian, L.; Tseng, T.; Holloway, P. H. Quantum Dots and Their Multimodal Applications: A Review. *Materials* **2010,** 3, 2260–2345.

11. Chuang, C. M.; Brown, P. R.; Bulović, V.; Bawendi, M. G. Improved performance and stability in quantum dot solar cells through band alignment engineering. *Nature Materials* **2014,** 13, 796-801.

12. Guldi, D. M.; Rahman, G. M. A.; Sgobba, V.; Kotov, N. A.; Bonifazi, D.; Prato, M. CNT−CdTe Versatile Donor−Acceptor Nanohybrids. *Journal of the American Chemical Society* **2006,** 128, 2315-2323.

13. The National Renewable Energy Laboratory Best Research-Cell Efficiency Chart. *https://www.nrel.gov/pv/cell-efficiency.html* (accessed Sept 10, 2019)

14. Anc, M. J.; Pickett, N. L.; Gresty, N. C.; Harris, J. L.; Mishra, K. C. Progress in Non-Cd Quantum Dot Development for Lighting Applications. *Journal of Solid State Science and Technology* **2013,** *2*, 3071-3082.

15. Zhou, J.; Yang, Y.; Zhang, C. Toward Biocompatible Semiconductor Quantum Dots: From Biosynthesis and Bioconjugation to Biomedical Application. *Chemical Reviews* **2015,** *115*, 11669-11717.

16. Regulacio, M. D.; Win, K. Y.; Lo, S. L.; Zhang, S.; Zhang, X.; Wang, S.; Han, M.; Zheng, Y. Aqueous synthesis of highly luminescent AgInS2–ZnS quantum dots and their biological applications. *Nanoscale* **2013,** 5, 2322-2327.

17. Walton Jarred LG demos Nano Cell technology displays. *https://www.pcgamer.com/lg-demos-nano-cell-technology-displays/* (accessed Oct 21, 2019)

18. Brunetti, V.; Chibli, H.; Fiammengo, R.; Galeone, A.; Malvindi, M. A.; Vecchio, G.; Cingolani, R.; Nadeau, J. L.; Pompa, P. P. InP/ZnS as a safer alternative to CdSe/ZnS core/shell quantum dots: in vitro and in vivo toxicity assessment. *Nanoscale* **2013,** *5*, 307-317.

19. Li, D.; Kristal, B.; Wang, Y.; Feng, J.; Lu, Z.; Yu, G.; Chen, Z.; Li, Y.; Li, X.; Xu, X. Enhanced Efficiency of InP-Based Red Quantum Dot Light-Emitting Diodes. *ACS Applied Materials and Interfaces* **2019,** *11*, 34067-34075.
20. Ekimov, A. I.; Onushchenko, A. A. Quantum size effect in three-dimensional microscopic semiconductor crystals. *Journal of Experimental and Theoretical Physics Letters* **1981,** *34*, 345-348.
21. Ekimov, A. I.; Efros, A. L.; Onushchenko, A. A. Quantum size effect in semiconductor microcrystals. *Solid State Communications.* **1985,** *56*, 921-924.
22. Reed, M. A.; Randall, J. N.; Aggarwal, R. J.; Matyi, R. J.; Moore, T. M.; Wetsel, A. E. Observation of discrete electronic states in a zero-dimensional semiconductor nanostructure. *Physical Review Letters* **1988,** *60*, 535-537.
23. Esaki, L. In *Semiconductor Superlattices and Quantum Wells through Development of Molecular Beam Epitaxy;* Chang, L. L., Ploog, K., Eds.; Molecular Beam Epitaxy and Heterostructures; Springer Netherlands: Dordrecht, 1985; pp 1-36.
24. NATO Advanced Study Institute on Molecular Beam Epitaxy (MBE) and Heterostructures, Chang, L. L., Ploog, K., North Atlantic Treaty Organization.,Scientific Affairs Division., *In Molecular beam epitaxy and heterostructures;* M. Nijhoff: Dordrecht; Boston, 1985.
25. Lianos, P.; Thomas, J. K. Cadmium sulfide of small dimensions produced in inverted micelles. *Chemical Physics Letters* **1986,** *125*, 299-302.
26. Steigerwald, M. L.; Alivisatos, A. P.; Gibson, J. M.; Harris, T. D.; Kortan, R.; Muller, A. J.; Thayer, A. M.; Duncan, T. M.; Douglass, D. C.; Brus, L. E. Surface derivatization and isolation of semiconductor cluster molecules. *Journal of the American Chemical Society* **1988,** *110*, 3046-3050.

27. Murray, C. B.; Norris, D. J.; Bawendi, M. G. Synthesis and characterization of nearly monodisperse CdE (E = sulfur, selenium, tellurium) semiconductor nanocrystallites. *Journal of the American Chemical Society* **1993,** *115*, 8706-8715.

28. Xie, R.; Zhang, J.; Zhao, F.; Yang, W.; Peng, X. Synthesis of Monodisperse, Highly Emissive, and Size-Tunable Cd_3P_2 Nanocrystals. *Chemistry of Materials* **2010,** *22*, 3820-3822.

29. Wu, D.; Kordesch, M. E.; Van Patten, P. G. A New Class of Capping Ligands for CdSe Nanocrystal Synthesis. *Chemistry of Materials* **2005,** *17*, 6436-6441.

30. L. L. Chang; K. Ploog Molecular Beam Epitaxy and Heterostructures; NATO Science Series E; 1985.

31. Pinczolits, M.; Springholz, G.; Bauer, G. Direct formation of self-assembled quantum dots under tensile strain by heteroepitaxy of PbSe on PbTe (111). *Applied Physics Letters* **1998,** *73*, 250-252.

32. Alchalabi, K.; Zimin, D.; Kostorz, G.; Zogg, H. Self-Assembled Semiconductor Quantum Dots with Nearly Uniform Sizes. *Physical Review Letters* **2003,** *90*, 026104.

33. Mews, A.; Eychmueller, A.; Giersig, M.; Schooss, D.; Weller, H. Preparation, characterization, and photophysics of the quantum dot quantum well system cadmium sulfide/mercury sulfide/cadmium sulfide. *Journal of Physical Chemistry* **1994,** *98*, 934-941.

34. Taleb, A.; Petit, C.; Pileni, M. P. Synthesis of Highly Monodisperse Silver Nanoparticles from AOT Reverse Micelles: A Way to 2D and 3D Self-Organization. *Chemistry of Materials* **1997,** *9*, 950-959.

35. Liu, J.; Raveendran, P.; Shervani, Z.; Ikushima, Y.; Hakuta, Y. Synthesis of Ag and AgI Quantum Dots in AOT-Stabilized Water-in-CO_2 Microemulsions. *Chemistry – A European Journal* **2005,** *11*, 1854-1860.

36. Alivisatos, A. P. Perspectives on the Physical Chemistry of Semiconductor Nanocrystals. *Journal of Physical Chemistry* **1996,** *100*, 13226-13239.

37. Xie, R.; Battaglia, D.; Peng, X. Colloidal InP Nanocrystals as Efficient Emitters Covering Blue to Near-Infrared. *Journal of the American Chemical Society* **2007,** *129*, 15432-15433.

38. Brichkin, S. B. Synthesis and properties of colloidal indium phosphide quantum dots. *Colloid Journal* **2015,** *77*, 393-403.

39. De Trizio, L.; Manna, L. Forging Colloidal Nanostructures via Cation Exchange Reactions. *Chemical Reviews* **2016,** 116, 10852-10887.

40. Reed, M. A. Vertical electronic transport in novel semiconductor heterojunction structures. *Superlattices and Microstructures* **1988,** *4*, 741-747.

41. Tisdale, W. A.; Zhu, X. -. Artificial atoms on semiconductor surfaces. *National Academy Science USA* **2011,** *108*, 965-970.

42. Zhou, H. S.; Sasahara, H.; Honma, I.; Komiyama, H.; Haus, J. W. Coated Semiconductor Nanoparticles: The CdS/PbS System's Photoluminescence Properties. *Chemistry of Materials* **1994,** *6*, 1534-1541.

43. Son, D. H.; Hughes, S. M.; Yin, Y.; Paul Alivisatos, A. Cation Exchange Reactions in Ionic Nanocrystals. *Science* **2004,** 306, 1009-1012.

44. Dorn, A.; Allen, P. M.; Harris, D. K.; Bawendi, M. G. In Situ Electrical Monitoring of Cation Exchange in Nanowires. *Nano Letters* **2010,** *10*, 3948-3951.

45. De Trizio, L.; Li, H.; Casu, A.; Genovese, A.; Sathya, A.; Messina, G. C.; Manna, L. Sn Cation Valency Dependence in Cation Exchange Reactions Involving Cu2-xSe Nanocrystals. *Journal of the American Chemical Society* **2014,** *136*, 16277-16284.

46. Shao, H.; Wang, C.; Xu, S.; Wang, Z.; Yin, H.; Cui, Y. Fast Doping of Cu into ZnSe NCs by Hydrazine Promoted Cation Exchange in Aqueous Solution at Room Temperature. Journal of Fluorescence **2015,** 25, 305−310.

47. De Trizio, L.; Gaspari, R.; Bertoni, G.; Kriegel, I.; Moretti, L.; Scotognella, F.; Maserati, L.; Zhang, Y.; Messina, G. C.; Prato, M.; et al. $Cu_{3-x}P$ Nanocrystals as a Material Platform for Near-Infrared Plasmonics and Cation Exchange Reactions. *Chemistry of Materials* **2015,** 27, 1120−1128.

48. Jessy B. R.; Prashant K. J. Cation exchange on the nanoscale: an emerging technique for new material synthesis, device fabrication, and chemical sensing. *Chemical Society Reviews* **2013,** 42, 89-96.

49. Parr, R. G.; Pearson, R. G. Absolute hardness: companion parameter to absolute electronegativity. *Journal of the American Chemical Society* **1983,** 105, 7512−7516.

50. Crabtree, R. H. *The Organometallic Chemistry of the Transition Metals;* A John Wiley & Sons, Inc.: 2004; pp 21-27.

51. Steinfeld I. J.; Francisco S. J.; Hase L. W. *Chemical Kinetics And Dynamics;* Prentice Hall Inc: 1999; pp 1-143.

52. Shao, H.; Wang, C.; Xu, S.; Jiang, Y.; Shao, Y.; Bo, F.; Wang, Z.; Cui, Y. Hydrazine-promoted sequential cation exchange: a novel synthesis method for doped ternary semiconductor nanocrystals with tunable emission. *Nanotechnology* **2013,** *25*, 025603.

53. Kim, S.; Marshall, A. R.; Kroupa, D. M.; Miller, E. M.; Luther, J. M.; Jeong, S.; Beard, M. C. Air-Stable and Efficient PbSe Quantum-Dot Solar Cells Based upon ZnSe to PbSe Cation-Exchanged Quantum Dots. *ACS Nano* **2015,** *9*, 8157-8164.

54. Bothe, C.; Kornowski, A.; Tornatzky, H.; Schmidtke, C.; Lange, H.; Maultzsch, J.; Weller, H. Solid-State Chemistry on the Nanoscale: Ion Transport through Interstitial Sites or Vacancies? *Angewandte Chemie International Edition* **2015,** *54*, 14183-14186.

55. Guo, Z.; Su, Y.; Li, Y.; Li, G.; Huang, X. Porous Single-Crystalline CdSe Nanobelts: Cation-Exchange Synthesis and Highly Selective Photoelectric Sensing toward Cu^{2+}. *Chemistry: A European Journal* **2018,** *24*, 9877-9883.

56. Heinz-Helmut; Perkampus; Grinter, H. C.; Threlfall, T. L. *UV-VIS Spectroscopy and Its Applications (Springer Lab Manuals);* Springer: 1994; pp 3-9.

57. Scott, R. A.; Lukehart, C. M., Eds.; In *Applications of Physical Methods to Inorganic and Bioinorganic Chemistry;* John Wiley & Sons Ltd: 2007; pp 529-536.

58. Hines, M. A.; Guyot-Sionnest, P. Synthesis and Characterization of Strongly Luminescing ZnS-Capped CdSe Nanocrystals. *Journal of Physical Chemistry* **1996,** *100*, 468-471.

59. Li, L. S.; Pradhan, N.; Wang, Y.; Peng, X. High Quality ZnSe and ZnS Nanocrystals Formed by Activating Zinc Carboxylate Precursors. *Nano Letters* **2004,** *4*, 2261-2264.

60. Chen, H.; Lo, B.; Hwang, J.; Chang, G.; Chen, C.; Tasi, S.; Wang, S. J. Colloidal ZnSe, ZnSe/ZnS, and ZnSe/ZnSeS Quantum Dots Synthesized from ZnO. *Journal of Physical Chemistry B* **2004,** *108*, 17119-17123.

61. Groeneveld, E.; Witteman, L.; Lefferts, M.; Ke, X.; Bals, S.; Van Tendeloo, G.; de, M. D. Tailoring ZnSe–CdSe Colloidal Quantum Dots via Cation Exchange: From Core/Shell to Alloy Nanocrystals. *ACS Nano* **2013,** *7*, 7913-7930.

62. Wang, A.; Shen, H.; Zang, S.; Lin, Q.; Wang, H.; Qian, L.; Niu, J.; Song Li, L. Bright, efficient, and color-stable violet ZnSe-based quantum dot light-emitting diodes. *Nanoscale* **2015,** *7*, 2951-2959.

63. Yu, W. W.; Qu, L.; Guo, W.; Peng, X. Experimental Determination of the Extinction Coefficient of CdTe, CdSe, and CdS Nanocrystals. *Chemistry of Materials* **2003,** *15*, 2854-2860.

64. Budennaya, L. D.; Nizkova, A. I.; Pekar, G. S.; Polisski, G. N. *Inorganic Materials* **1982,** *18*, 760-764.

65. Morris, A. L.; Lin, C.; Benjamin, S. E.; Devarasetty, V. V. N. M.; Tilluck, W. R.; Lozano, E. I.; Hamo, H.; Aguilar, X. A.; Van Patten, P. G. Toward Improved Scalability of Cation Exchange Reactions of Metal Chalcogenide Nanocrystals. Chemistry of Materials **2017,** 29, 6596-6600.

66. Oliveria, M.; McMullan, R. K.; Wuensch, B. J. *Solid State Ionics* **1988,** *28*, 1332-1337.

67. Gui, J.; Ji, M.; Liu, J.; Xu, M.; Zhang, J.; Zhu, H. Phosphine-Initiated Cation Exchange for Precisely Tailoring Composition and Properties of Semiconductor Nanostructures: Old Concept, New Applications. Angewandte Chemie International Edition **2015,** 54, 3683−3687.

68. Santangelo, S. A.; Hinds, E. A.; Vlaskin, V. A.; Archer, P. I.; Gamelin, D. R. Bimodal Bond-Length Distributions in Cobalt-Doped CdSe, ZnSe, and $Cd_{1-x}Zn_xSe$ Quantum Dots. *Journal of the American Chemical Society* **2007,** *129*, 3973-3978.

69. Toh C. *Advanced Study Guide Chemistry;* Step-by-Step International Pte. Ltd: 2013; pp 57.

70. Yu, W. W.; Wang, Y. A.; Peng, X. Formation and Stability of Size-, Shape-, and Structure-Controlled CdTe Nanocrystals: Ligand Effects on Monomers and Nanocrystals. *Chemistry of Materials* **2003,** *15*, 4300-4308.

71. Luo, Y. Bond Dissociation Energies. *https://notendur.hi.is/agust/rannsoknir/papers/2010-91-CRC-BDEs-Tables.pdf* (accessed Oct 16, 2019).

72. Durán, G. M.; Plata, M. R.; Zougagh, M.; Contento, A. M.; Ríos, Á Microwave-assisted synthesis of water-soluble thiol capped CdSe/ZnS quantum dots and its interaction with sulfonylurea herbicides. *Journal of Colloid and Interface Science* **2014,** 428, 235-241.

APPENDICES

APPENDIX A

KINETIC MODELS EXPLORED

Several functions were investigated to fit the kinetic curves obtained from the stopped-flow kinetic instrument with the goal of achieving a good fit for better understanding of the rate of the cation exchange process in the quantum dots. Magic plot was employed for the fitting of the curves which generate a report with details of the quality of the kinetic curves fitting. The parameters that interprets the quality of the fitting include residual sum of squares (RSS, χ^2), reduced RRS, residual standard deviation (RSTDev), and coefficient of determination (R^2).

The kinetic models used include a sequential model, sum-of exponentials function, and single exponential function, and how these functions performed as a fit to the experimental data is reported using the parameters listed above. However, the function of choice for the fitting of the experimental data is not based on a specific mechanism, but rather that it gives a way to quantify the relative rate constants at the various stages of the cation exchange reaction.

A1.1 Functions and Reports

A1.1.1 ZnSe and CdSe Quantum Dots (QDs) Comparison

A1.1.1.1 CdSe Fitting

$$y = A * \{1 - \exp[-k_1(x)]\} + B * \{1 - \exp[-k_2(x)^{\beta}]\} + C * \{1 - \exp[-k_3(x)]\} + z \quad \text{A1.1}$$

$$y = A * \{1 - \exp[-k_1(x)]\} + B * \{1 - \exp[-k_2(x)]\} + C * \{1 - \exp[-k_3(x)]\} + z \quad \text{A1.2}$$

$$y = A * \{1 - \exp[-k_1(x)]\} + B * \{1 - \exp[-k_2(x)]\} + z \quad \text{A1.3}$$

$$y = A * \{1 - \exp[-k_1(x)^{\beta}]\} + z \quad \text{A1.4}$$

$$y = A * \{[B * (1 - \exp(-k_1(x - c)))] + [C * (1 - \exp(-k_2(x - c)))]\} \quad \text{A1.5}$$

Functions	RSS, χ^2	RSS	RSTDev	R^2
A1.1 (adopted)	0.0098	2.0226×10^{-5}	0.0045	0.9997
A1.2	0.0702	1.4533e-4	0.0121	0.9977
A1.3	0.0702	1.4443e-4	0.012	0.9977
A1.4	0.0618	1.2759e-4	0.0113	0.998
A1.5	0.0702	1.4563e-4	0.0121	0.9977

A1.1.2 Comparison of Different Capping-ligands

A1.1.2.1 Dodecylamine (DDA) Fitting

$$y = A * \{1 - \exp[-k_1(x)^{\beta}]\} + B * \{1 - \exp[-k_2(x)]\} + z \quad \text{A1.6}$$

$$y = A * \{1 - \exp[-k_1(x)]\} + B * \{1 - \exp[-k_2(x)]\} + z \quad \text{A1.7}$$

$$y = A * \{1 - \exp[-k_1(x)^{\beta}]\} + z \quad \text{A1.8}$$

$$y = A * \{1 - \exp[-k_1(x)]\} + z \quad \text{A1.9}$$

$$y = A * \{[B * (1 - \exp(-k_1(x - c)))] + [C * (1 - \exp(-k_2(x - c)))]\} \quad \text{A1.5}$$

Functions	RSS, χ^2	RSS	RSTDev	R^2
A1.6 (adopted)	0.0043	9.0236e-6	0.003	0.9997
A1.7	0.1569	3.3023e-4	0.0182	0.9893
A1.8	0.3878	8.1476e-4	0.0285	0.9735
A1.9	0.3879	8.1325e-4	0.0285	0.9735
A1.5	0.1569	3.3093e-4	0.0182	0.9893